Journal of Structural Geology, Vol. 13, No. 6, pp. 691 to 710, 1991
Printed in Great Britain

0191-8141/91 $03.00+0.00

Thrust-related strain gradients and thrusting mechanisms in a chevron-folded sequence, southeastern Australia

DAVID R. GRAY and CLIVE E. WILLMAN*

Department of Earth Sciences, Monash University, Melbourne, Victoria 3168, Australia

(*Received* 29 *June* 1990; *accepted in revised form* 28 *December* 1990)

Abstract—An E-directed, imbricate-fan thrust-system within a chevron-folded, monotonous quartz-rich turbidite succession shows marked gradients in strain from the upper to lower parts of individual thrust-sheets. Upper parts of thrust-sheets show low to moderate strains (XZ strains < 5.0:1), subvertical extensions defined by straight quartz-fibres in pressure-shadows on framboidal pyrite, and 50–65% shortening in the inferred thrust-transport direction. This shortening is reflected by upright, close chevron-folds (ILA ≈ 35–50°, where ILA is fold interlimb angle) with axial lines subparallel to major fault traces, spaced cleavage and both E- and W-dipping reverse faults. Lower parts of thrust-sheets are characterized by high strains (XZ > 30:1), tight inclined chevron folds (ILA < 30°) with predominantly W-dipping axial surfaces, intense phyllitic cleavage with a strong down-dip mineral stretching lineation, and long curved tapering quartz pressure-shadows on pyrite. Such differences in fold geometry, the intensity of the cleavage and the geometry of quartz-fibres in pressure shadows, require thrust-sheet emplacement to be synchronous with the internal deformation of sheets. Thrust-sheets show a change from an approximately constant volume, plane strain coaxial deformation in their upper parts to non-coaxial high strain deformation with incremental (ω_i) between those expected for pure shear and simple shear (i.e. $0 < \omega_i < 5.45°$) in their basal parts. Observed geometries and intensities reflect partitioning of strain and deformation mechanisms within individual thrust-sheet volumes both during the initiation and propagation of subsurface detachment-faults, and with their emplacement to shallower crustal levels. Strain softening, related to chevron-folding and more intense cleavage development within a 500 m basal zone, has controlled the emplacement of these turbidite-dominated thrust-sheets. Transport and internal deformation of the thrust-sheets did not involve gravitationally-induced spreading, but required either a push from the rear or some form of underthrusting.

INTRODUCTION

STRUCTURES within thrust-sheets reflect the accumulation of strains during their emplacement to shallower crustal levels and their interaction with other thrust-sheets subsequent to emplacement (e.g. Elliott 1976, Mitra & Elliott 1980, Coward & Kim 1981, Sanderson 1982, Geiser 1988). Knowledge of the internal deformation of individual thrust-sheets is therefore important for understanding thrusting-emplacement mechanisms and for defining the emplacement history of individual thrust-nappes. Thrust emplacement shows a spectrum of behaviour between end-member models of rigid and viscous gliding (Brun & Merle 1985, Merle 1986). Rigid gliding models require frictional sliding of a rigid block over a footwall with little or no penetrative deformation in the hanging wall (Wojtal 1986). At the other extreme, viscous gliding requires displacement by ductile-yield in the hangingwall which is reflected by penetrative deformation of the sheet particularly towards the base. Extreme localization of deformation at the base of thrust-sheets can occur (e.g. Schmid 1975, Mitra 1984, Gilotti & Kumpulainen 1986), but widely distributed deformation in thrust hanging walls is also common (Geiser 1988). Such deformation generally causes overall thickening of the thrust-sheet accompanied by shortening of the sheet in the transport direction.

This paper investigates hanging wall deformation of thrust-sheets within part of the Tasman orogenic belt of southeastern Australia (Fig. 1). The region provides an opportunity to assess the internal deformation of thrust-sheets in rocks other than the largely carbonate platform sequences of the classic thrust belts of the Appalachian and the Rocky Mountain orogens. In the Ballarat Slate Belt of central Victoria a deformed quartz-rich turbidite sequence shows regional-scale regularity of upright chevron-folding associated with steeply dipping reverse faults. Recent deep-crustal seismic reflection profiling (Gray *et al.* in press) has shown that these reverse faults flatten with depth and have listric form. Overall shortening (>60%) within the quartz-rich turbidite succession requires detachment from the underlying Cambrian metavolcanics and allochthoneity of the sequence (Cox *et al.* 1983, Gray & Willman 1985, 1991, Fergusson *et al.* 1986, Gray 1988).

The internal geometry of individual thrust-sheets in the Ballarat Slate Belt is linked to their displacement history. Structures in the immediate hanging wall are attributed to distributed shear strain in the lower 2–3 km of the sheets, a region which constitutes approximately 20–30% of their total thicknesses. The overall geometry of the belt and the general structural relationships are described elsewhere (Gray & Willman 1991).

GEOMETRY OF THE THRUST-BELT

Regional setting

The thrust-belt is centrally situated in the southern part of the Lachlan Fold Belt, within the N–S-trending

*Present address: Victorian Geological Survey, Bendigo, Victoria 3550, Australia.

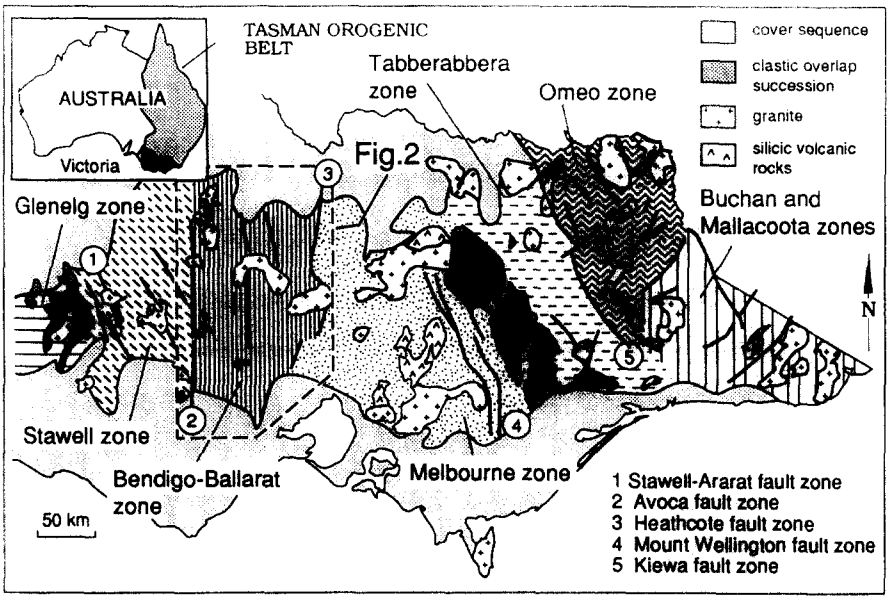

Fig. 1. Geological map of Victoria showing the major structural zones and the major faults within this part of the Palaeozoic Lachlan Fold Belt.

composite Palaeozoic Tasman orogenic belt along the eastern margin of Australia (Fig. 1). The Lachlan Fold Belt consists of a number of fault-defined structural zones which represent accreted fragments of an Early Palaeozoic submarine fan system along the Gondwana margin (cf. Fergusson *et al.* 1986, Gray 1988). The structural zones, although having similar lithology and structural style, show differences in the timing of deformation and different structural trends (Fig. 1). The monotonous succession of Ordovician through Devonian quartz-rich turbidites is laterally extensive over the 800 km present-width with an approximate thickness upwards of 10 km. Linear fault-bounded belts of Cambrian greenstones (metavolcanics) which comprise boninites, low Ti andesites and tholeiites of oceanic affinities, separate many of the zones and are considered to underlie the quartz-rich turbidite succession (Crawford & Keays 1978).

The Mount Wellington fault zone (Fig. 1) is a major upper-crustal structural discontinuity that separates fold-thrust zones of different age and vergence. The Ballarat Slate Belt (Bendigo–Ballarat zone: Fig. 1) is part of a post-Silurian (*Tabberabberan* event) E-vergent fold–thrust belt which possibly includes the Stawell, Bendigo–Ballarat and Melbourne zones (Fig. 1). East of the Mount Wellington fault zone the Tabberabbera and Omeo zones (Fig. 1) are part of an Early Silurian (*Benambran* event) SW-vergent thrust-belt (Fergusson *et al.* 1986). Thin skinned deformation involving a mid-crustal level detachment between the base of the Ordovician and the top of the Cambrian, has been proposed for the Lachlan Fold Belt on the basis of the overall shortening in the quartz-rich turbidite sequence (60–70% Bendigo–Ballarat zone; 50% Melbourne zone), the character of the Stawell, Heathcote and Mount Wellington fault zones, the W-dipping and older over younger rocks along the major faults, the apparent diachroneity of the deformation from west to east, and the mixed character of the I and S type granites (cf. Fergusson *et al.* 1986, Gray 1988). The lack of coincidence between basement terranes based on granite petrogenesis (Chappell *et al.* 1988) and tectonostratigraphic terranes (Fergusson *et al.* 1986) and structural zones (Gray 1988) requires a composite layered crust for the Lachlan Fold Belt in Victorian with the lower crust probably thinned Proterozoic continental crust. However, thrust slices or windows exposing Proterozoic basement within the Lachlan Fold Belt are not observed on the Australian mainland.

The thrust-belt is coincident with the Bendigo–Ballarat zone (Gray 1988), a 110 km wide zone of folded, cleaved and faulted Ordovician quartz-rich turbidites between the Avoca fault zone on the west and the Heathcote fault zone on the east (Fig. 2). It is a grossly inhomogeneous sequence of interbedded quartz-wacke turbidites, siltstone and mudstone with marked lateral and vertical facies changes (see Cas & VandenBerg 1988). Despite the lack of a recognizable stratigraphy within the quartz-rich turbidite succession, abundant graptolite fauna within black mudstones have made it possible to use biostratigraphic zonation to define regional structural relationships (Harris & Thomas 1938, Thomas 1939, Hills & Thomas 1954).

The Ordovician rocks are intruded by Late Devonian granitoids and are locally unconformably overlain by a gently folded unfossiliferous sandstone and conglomerate sequence of possible Upper Devonian age (Fig. 2). Deformation in the Ballarat Slate belt is considered Early–Middle Devonian in age (*Tabberabberan* event) as constrained by the post-tectonic Late Devonian granitoid intrusives and the deposition of the Upper Devonian overlap succession (Cas & VandenBerg 1988, Gray 1988, Gray & Willman 1991). The granites are mainly post-tectonic and are younger in the east (360 ± 8 Ma) than those in the west (390 ± 7 Ma) which show some syn-tectonic character in their aureoles (Richards &

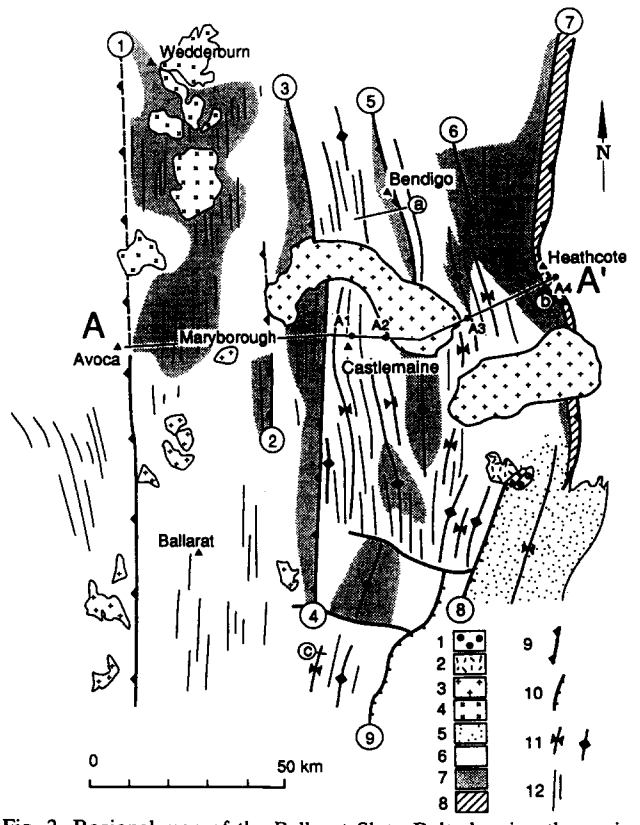

Fig. 2. Regional map of the Ballarat Slate Belt showing the major structural elements and gross stratigraphic relationships. Circled numbers are major fault traces: ① Avoca fault zone; ② Campbelltown fault; ③ Leichardt fault; ④ Muckleford fault; ⑤ Whitelaw fault; ⑥ Fosterville fault; ⑦ Heathcote fault zone; ⑧ Djerriwarrh fault; and ⑨ Rowsley East fault. Locations of cross-sections referred to in the text are shown as A–A′: regional structural profile (Fig. 3a) ⓐ Bendigo (Fig. 6a); ⓑ Red Hill, Heathcote (Fig. 7a); and ⓒ Moorabool River (Fig. 10a). Legend symbols are: 1, continental clastic overlap succession; 2, Late Devonian silicic volcanics; 3, Late Devonian granitoids; 4, Early Devonian granitoids; 5, Middle–Upper Ordovician quartz-rich turbidites; 6, Middle–Lower Ordovician quartz-rich turbidites; 7, Lancefieldian (lowermost Lower Ordovician) quartz-rich turbidites; 8, Cambrian metavolcanics and volcaniclastics; 9, reverse fault outcrop trace; 10, extension fault outcrop trace; 11, synclinorial and anticlinorial axial surface traces; 12, structural trend lines.

Singleton 1981). If granite generation is a consequence of the deformation then the deformation should be diachronous across the belt.

Thrust-belt geometry

Major W-dipping, meridional strike-parallel contraction faults dominate the surface geology (Fig. 2) and probably reflect a leading-imbricate fan thrust-system in the subsurface (Fig. 3). At the present level of exposure these faults all dip at 60° or greater (Fig. 3a), but are considered to have listric form and flatten with depth as suggested by deep crustal seismic profiling of the Heathcote fault zone (Fig. 3b) (Gray *et al.* in press). The faults truncate meridional regional anticlinoria and synclinoria and generally place lowermost Ordovician (Lancefieldian) over either uppermost Lower Ordovician (Chewtonian–Castlemainian) or Middle Ordovician (Darriwilian–Yapeenian) rocks. Structural trends are NNW (335–345°) in the northern part of the belt with a gradual swing to either N or NNE (020–035°) in the southern part (Fig. 2). There is structural similarity from north to south, although the major strike-faults are more common in the north. Palinspastic restoration of the zone gives an original width of approximately 370 km compared to the present width of 110 km.

Regional folds have wavelengths of 10–15 km and amplitudes in the order of 1–2 km. Within individual thrust-sheets there is a general westward younging in the stratigraphy and a gentle westerly dip of the regional fold enveloping surface (Fig. 3a). Regional folds show pronounced domal culminations and basinal depressions characterized by marked plunge changes (Fig. 2). Domal culminations, particularly south of the Harcourt granite between the Muckleford and Heathcote fault zones, have been inferred from graptolite biostratigraphic zones as NNE-trending, en échelon oval to canoe-shaped outcrop patterns of Lancefieldian rocks (Thomas 1939).

Three major lithotectonic units define the overall stratigraphic column in central Victoria and include the Ordovician package (approximately 3 km thickness), the Upper Cambrian shales and cherts (900 m maximum thickness) and the Mid- to Lower Cambrian volcanics and volcaniclastics (2–2.5 km thickness) (Gray & Willman 1991). The westerly dip of the major faults, their juxtaposition of older rocks over younger rocks and the presence of Lowermost Ordovician (Lancefieldian) in their immediate hanging walls suggests fault propagation and detachment in the Lancefieldian associated with an easterly transport of the folded and telescoped cover over the underlying Cambrian metavolcanic succession. Horses of Cambrian within the Heathcote fault zone, the leading fault, suggest duplexing and serial detachment in the Cambrian succession.

Inferred detachments are at 4–6 km depth within the Lancefieldian or Lower Ordovician (with the Campbelltown, Muckleford and Whitelaw faults as splays off this) and at 7–10 km depth within the lower part of the Cambrian succession (Heathcote fault zone). The lack of topographic relief, structural relief (e.g. culminations) produced by folding of thrusts, and extensive deep-crustal seismic relection profiling makes it difficult to decipher the three dimensional geometry of the fault network in the subsurface. All crustal sections (e.g. Fig. 3b) can therefore only be considered as speculative at this stage.

Nature of the faults

All faults are brittle–ductile faults characterized by knife-sharp discontinuities with occasional cataclastic material or clayey gouge (pug). They commonly have associated high strain zones of varying widths (up to 4 km) showing intense development of crenulation cleavages associated with variably, but generally steeply plunging meso- and micro-folds. Overprinting cleavages within these zones indicate complex fault movements with early thrusting (D_1) followed by dextral movement (D_2) followed by weak sinistral movement (D_3) (Gray & Willman 1991); localized NW-trending crenulation

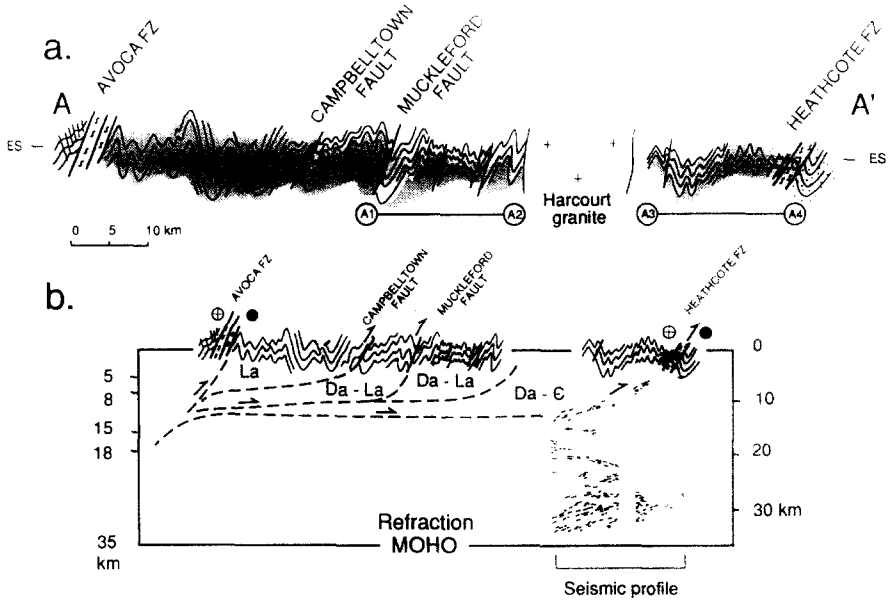

Fig. 3. Regional geometry of the thrust-belt. (a) Structural profile across the Ballarat Slate Belt based on the surface geology; ES specifies the present level of the essentially flat erosion surface. The shaded segments represent the Lowermost Ordovician (Lancefieldian) and the stipple are Siluro-Devonian rocks of the Melbourne zone. A1–A2: Castlemaine structural profile and A3–A4: Heathcote structural profile (see Table 1). (b) Speculative crustal profile incorporating both surface geology and deep seismic reflection profiling data (cf. Gray *et al.* in press). Inferred strike-slip movement components on the major bounding faults are shown by +, indicating block movement out of the page, and O indicating movement into the page. Stratigraphic intervals represented within each thrust-sheet are shown; La, Lancefieldian (Lowermost Ordovician); Da, Darriwilian (Middle Ordovician); and C, Cambrian.

cleavages reflect the dextral movement, whereas overprinting NE-trending crenulation cleavages reflect the later weak sinistral movement.

The major bounding faults are the Avoca and Heathcote fault zones with widths of 2–4 km and lengths in excess of 100 km (Fig. 1). The Avoca fault zone has a linear N-trending trace which separates NW-trending Cambro-Ordovician rocks of the Stawell zone, from the N-trending Lower Ordovician (Lancefieldian) rocks of the Bendigo–Ballarat zone (Fig. 2). The Heathcote fault zone juxtaposes Cambrian metavolcanics and volcaniclastic rocks of the Bendigo–Ballarat zone with Devonian quartz-rich turbidites of the Melbourne zone. In the north the Heathcote fault zone consists of two faults which bound the outcrop of the Cambrian succession, whereas to the south it is a single fault which loses stratigraphic displacement within the Upper Ordovician sequence (Fig. 2). It shows a bend and accompanying structural complexity at Heathcote.

Major strike-parallel faults have linear map traces from 25 to 100 km in length and generally dip at 60–70° W. They include the Campbelltown, Leichardt, Muckleford, Sebastian and Whitelaw faults. Minor faults (throws of less than 100 m) are abundant throughout the zone and show both dips to the east and to the west. Northwest- and NE-trending cross-faults, generally with strike displacements of metres to tens of metres are also present within the zone (Fig. 2).

INTERNAL GEOMETRY OF THRUST-SHEETS

Thrust-sheets in the Bendigo Slate Belt are tightly folded, cleaved and cut by numerous minor faults and show horizontal shortenings in the order of 60–70% (Table 1). Fold geometry, cleavage intensity, lineation development and total strain magnitude vary with structural position within individual thrust-sheets. The basal parts of thrust-sheets have different internal geometries than their upper parts, as exemplified by chevron-fold geometry, the nature and intensity of cleavage, total strain magnitude and syn-tectonic fibres in pressure shadows on pyrite (Figs. 4 and 5).

Nature of the chevron folding

All thrust-sheets consist of extremely regular, parallel trains of gently plunging, upright, angular chevron folds (Fig. 3a), with their axial surface traces showing strike-lengths in the order of tens of kilometres (Fig. 2). They have steep, N–S-trending axial surfaces with doubly plunging axes producing both regional and local culminations and depressions. Neighbouring folds may merge horizontally and vertically to form zones of monoclinal flexure which eventually die out on the limbs of major host folds. Axial surface traces of parasitic folds are spaced at approximately 8 per km, defining several orders of folding with lower-order fold wavelengths ranging from 100 to 300 m and fold-amplitudes from 50 to 100 m (Gray & Willman 1991).

The folds have typical chevron form with long straight limbs and narrow hinge zones (Fig. 4a). Hinge geometry varies from rounded in sandstone dominated facies to angular in mudstone dominated sections. Limb-thrusts, bedded veins and saddle reefs are relatively common. Interlimb angles range from 18° to 70° with variations not only from section to section (Table 1), but within

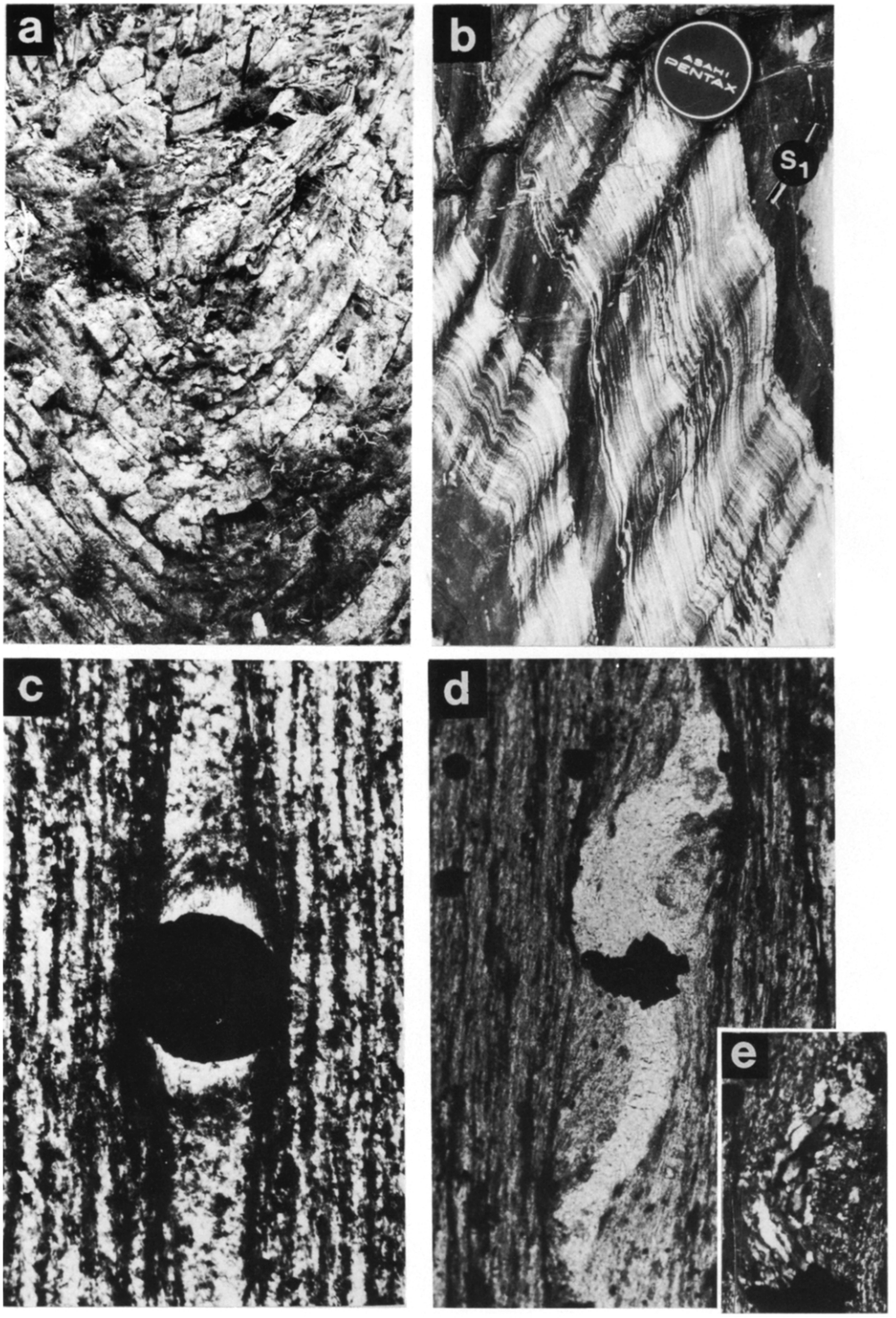

Fig. 4. Structural elements of the Ballarat Slate Belt. (a) Synclinal closure in amalgamated sandstone succession, Lerderderg gorge north of Bacchus Marsh. Width of photograph is approximately 20 m. (b) Crenulated and cleaved laminated siltstone and black mudstone, Chewton–Castlemaine railway line. S_1: primary crenulation cleavage. (c) Subspherical framboidal pyrite with straight, fibrous-quartz/white mica pressure shadow within slate. (Lerderderg River gorge, Bacchus Marsh; sample 84-19 D, Appendix 1.) Width of photograph is 700 μm. (d) Long curved quartz pressure shadows tails on pyrite within slates of the hanging wall to the Heathcote fault, Red Hill near Heathcote (PPL; Sample 88-197, Appendix 1). Width of photograph is 800 μm. (e) Crossed-polars view of part of the pressure shadow in (c) showing the marked recovery and recrystallization of the originally curved blade-like quartz-fibres.

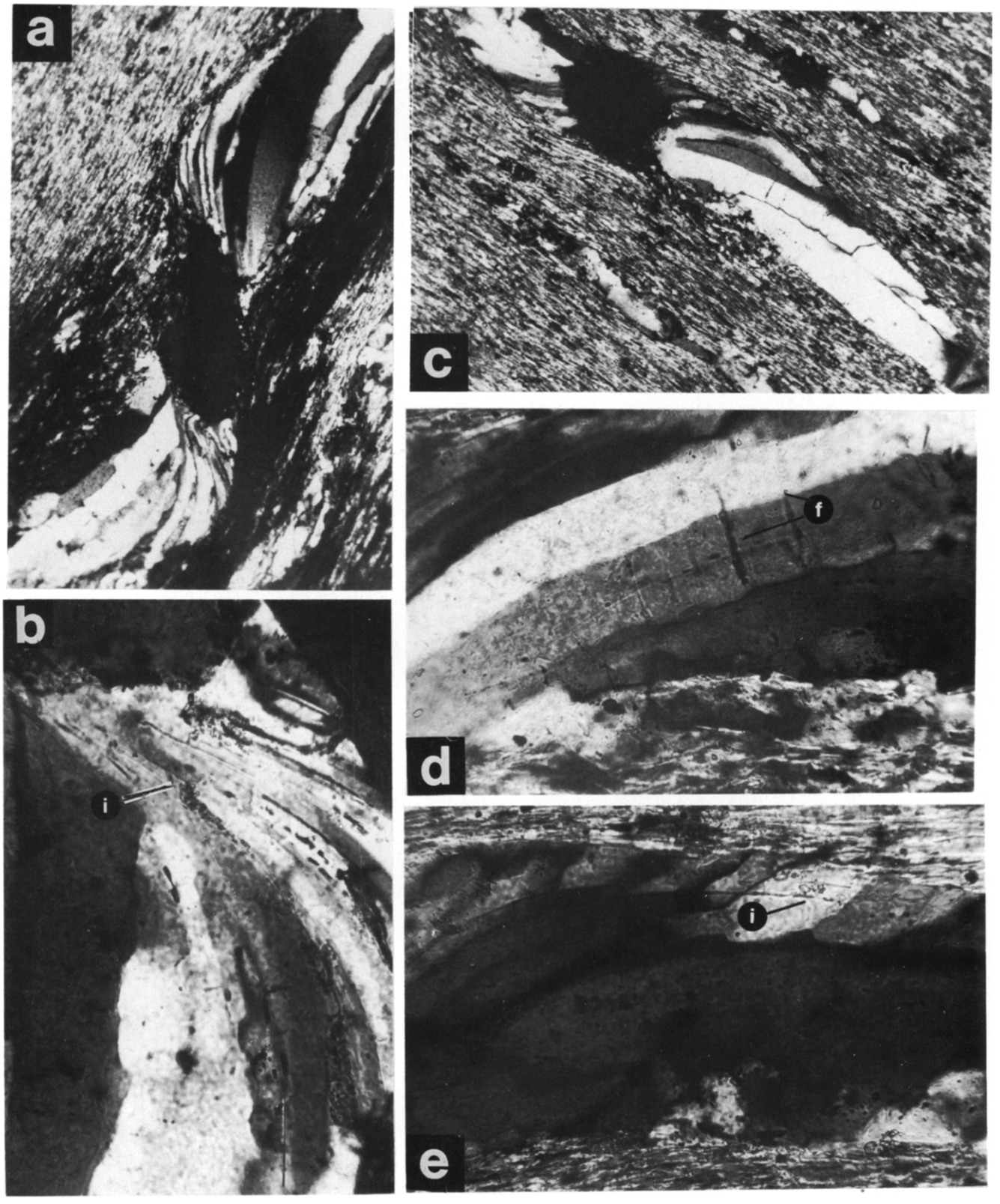

Fig. 5. Morphology of pressure shadows with long curved, bladed quartz-fibres from the hanging wall of the Whitelaw fault, Bendigo (sample 84-131; Appendix 1). (a) Varying fibre morphology and partition line within long, curved, asymmetric pressure shadow on pyrite. Width of photograph is 800 μm. (b) Enlargement of (a) showing the fibrous morphology of quartz near the interface with the pyrite. Note the ghost-fibre inclusion trails (**i**) parallel to individual quartz-fibres and the bulge-like grain boundaries between some of the fibres. Width of photograph is 180 μm. (c) Asymmetric quartz pressure-shadow showing marked variation in 'fibre' width across the pressure shadow. Width of photograph is 800 μm. (d) Enlargement of (c) showing healed-fractures (**f**) orthogonal to fibre boundaries. Width of photograph is 180 μm. (e) Complex substructure within quartz 'fibres' overprinting relict ghost-fibre inclusion trails (**i**) which still preserve the original fibre-directions within deformed segments of the pressure shadows. Width of photograph is 180 μm.

Table 1. Components of shortening for the Ballarat Slate Belt

Structural profile	Total shortening e_t*		Fault shortening e_f*	Fold shortening e_{cf}*	Fold interlimb angle†
	m‡	c‡			
Bendigo§[1]	60.6%	60.5%	1.1%	60.1%	37.9° (15)
Heathcote§[2]	47.4%	47.4%	3.5%	45.5%	50.9° (18)
Castlemaine§[3]	51.3%	51.2%	4.4%	49.0%	37.9° (15)
Brisbane Ranges§[4]			‖	63.9%	35.1° (18)

*e (elongation) = $(l_1 - l_0)/l_0$, and l_1 is the deformed length and l_0 the undeformed length; and e_t is the total shortening including effects due to both folding and faulting; e_f is the shortening due to faulting; and e_{cf} is the shortening due to chevron folding alone (i.e. faults removed).

†Mean value with sample number in brackets.

‡m, measured total shortening; c, calculated total shortening, (Note: $(1 + e_t) = (1 + e_{cf})(1 + e_f)$ or $\ln e_t = \ln e_{cf} + \ln e_f$.)

§Section locations (superscripts): 1, ⓐ on Fig. 2; 2, A3–A4 on Fig. 2; 3, A1–A2 on Fig. 2; 4, ⓒ on Fig. 2.

‖Problem with superimposed normal faulting.

some sections as major faults are approached (Fig. 6). The Bendigo, Chewton–Castlemaine and Brisbane Ranges sections show the tightest folds with fold interlimb angles of 31°, 38° and 35°, respectively.

In the lower parts of thrust-sheets changes in fold tightness and dip/dip direction of the axial surfaces accompany marked increases in strain. The Bendigo section (Fig. 6a) shows increased fold tightness with an interlimb angle of 23° up to 3 km away from the Whitelaw fault, where the measured background fold interlimb angle is approximately 36° at 3–8 km distance from the fault trace (Fig. 6b). A similar change is also noted in the Chewton–Castlemaine section, but there is no mapped or known fault at the end of the section where the fold interlimb angle decreases (Fig. 3a, segments A1 and A2). Changes in fold axial surface attitude also accompany increasing fold tightness within these zones adjacent to the major faults. Dips of fold axial surfaces change progressively from a steep (>80°) east dip to a steep (>75°) west dip with decreasing fold interlimb angle (Fig. 6c). In the Heathcote section the average fold interlimb angle is 51° with no noticeable change as the Heathcote fault zone is approached. A zone of increased faulting and polydeformation with intense crenulation cleavage development which occurs up to 4 km from the Heathcote fault zone, has overprinted the

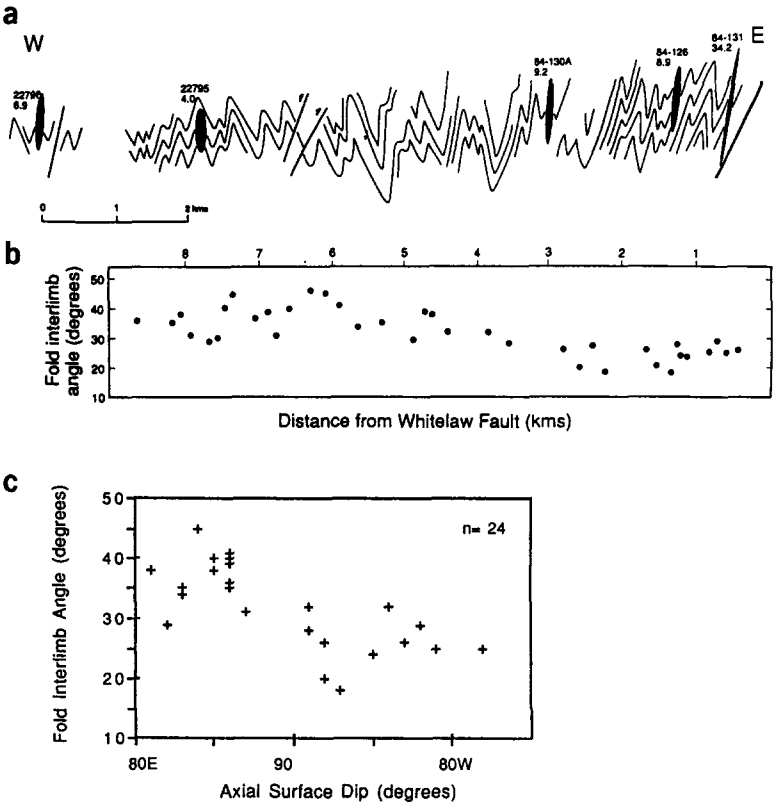

Fig. 6. Fold tightness variations across the Bendigo region to the Whitelaw fault (see a on Fig. 2 for location). (a) Structural profile showing bedding form lines and XZ strain ellipses; sample numbers and strain magnitude are given for each ellipse. (b) Graph showing fold interlimb angle (degrees) plotted against distance from the Whitelaw fault. (c) Fold interlimb angle (degrees) plotted against axial surface dip for folds in the structural profile in (a).

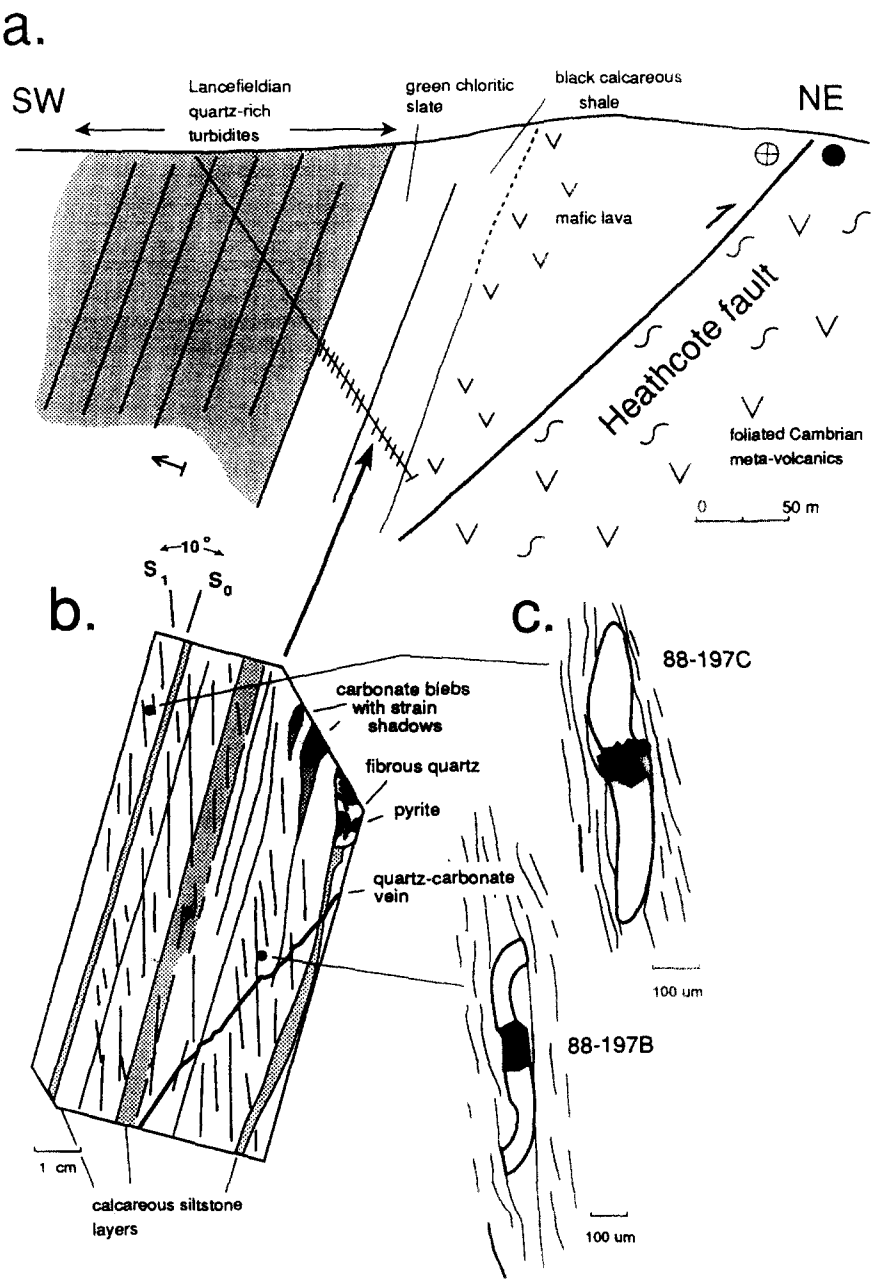

Fig. 7. Relationships of pressure shadows with curved fibres to other structural elements in the hanging wall of the Heathcote fault zone, Red Hill, Heathcote (see ⓒ on Fig. 2 for location). (a) Cross-section showing location of the sample from a diamond drillhole in a Cambro-Ordovician sequence of mafic lavas, black shales, green shales transitional into mudstone and sandstone. (b) Thin section sketch of black slate with calcareous siltstone bands and carbonate blebs with strain shadows. (c) Examples of curved pressure shadow tails on euhedral pyrites. Locations shown in (b).

early thrusting-related high strain zone. Evidence of this non-coaxial, high strain deformation has been found within interbedded black carbonaceous and green chloritic shales from drill core immediately above the Heathcote fault zone (Fig. 7).

Overturning of fold limbs is rare and has only been observed in the hanging walls of the Whitelaw and Heathcote faults. Overturned folds tend to be almost isoclinal and are cut by numerous minor faults.

Cleavage

Cleavage varies from divergent-fanning slaty cleavage or primary crenulation cleavage (Fig. 4b) in pelites to a convergent-fanning spaced cleavage in sandstones. The cleavages are typically thin spaced zones (M domains) of subparallel white mica and chlorite alternating with microlithons or intercleavage zones (Q domains) of quartz and white mica aggregates (Glasson & Keays 1978, Stephens *et al.* 1979). Abundant evidence of dissolution is shown by truncated quartz grains along cleavage, stripy differentiated layering, pressure shadows and mica beards (Glasson & Keays 1978, Stephens *et al.* 1979, Waldron & Sandiford 1989), although late stage movement on some cleavage surfaces has also caused fracturing of grains typical of cataclasis (White & Johnston 1981). Originally bulk rock chemistry was used to imply volume losses of 10–20% during cleavage

formation (Stephens *et al.* 1979), but approximately constant volume deformation for the Ballarat slates has recently been argued on both chemical and geometric grounds (Binns & Eames 1989, Waldron & Sandiford 1989).

In the structurally lower parts of individual thrust-sheets, that is, close to major faults (on the regional map scale) cleavage in pelitic layers is more intense with closer spacing of cleavage lamellae and very low bedding–cleavage angles ($S_0 \wedge S_1 < 20°$) (Fig. 7). In outcrop this cleavage has a distinct phyllitic sheen and shows a prominent down-dip stretching lineation generally due to strongly aligned, long quartz-tails in pressure shadows on pyrite. Crenulation cleavages are also locally developed reflecting polydeformation and folding of the regionally extensive first cleavage (S_1) within and adjacent to these fault zones.

Total strain magnitudes

Total strain in mudstones, determined largely from syn-tectonic quartz-fibres in pressure shadows on pyrite (Figs. 4c–e and 5) and graptolites on bedding planes (see Appendices 1 and 2), varies regionally across the thrust-belt (Fig. 8); 207 measurements of pressure shadows from 33 localities (Appendix 1) give direct values of the maximum principal stretch and enable calculation of the bulk XZ strain at individual localities, where X, Y and Z are the maximum, intermediate and minimum principal strains, respectively. Grouped regional data (Fig. 9) shows variable XZ strain ($2.0 > R \leq 50.0$), although in the Blackwood and Moorabool River (Brisbane Ranges) traverses XZ strains are relatively homogeneous. Background values appear between 2.0 and 5.0, and away from faults the strains in mudstones are relatively homogeneous. Higher strains occurred in the Lerderderg Gorge (CT5A) and Bendigo–Castlemaine (84-137) areas (see Appendix 1), but the highest strains ($XZ > 30:1$) are associated with the hanging walls of the major faults (e.g. 84-131 (Bendigo): Whitelaw fault, and 88-197 (Red Hill, Heathcote): Heathcote fault; see Appendix 1). There is no apparent correlation between high strains and the inferred domal culminations as has been observed in other slate belts, where greater vertical extension was associated with the culminations along fold axial lines (cf. Wood 1974).

XZ strain estimates in most regions vary with bedding–cleavage angle (Fig. 9); high values ($XZ > 30:1$) are associated with very low bedding–cleavage angles ($S_0 \wedge S_1 < 20°$) and reflect the decreased fold interlimb angles observed in the basal parts of thrust-sheets. Strain magnitude also varies with lithology, as XZ strains in sandstones determined by the Fry method (see Appendix 2) range between 1.3 and 1.7 (Appendix 1), and are significantly lower than those in mudstones. Psammites show XZ strain magnitude variations dependent on position on folds; XZ strain estimates from fold hinges are generally higher (≈1.6–1.7) than limb estimates (≈1.3) from the same fold (Appendix 1).

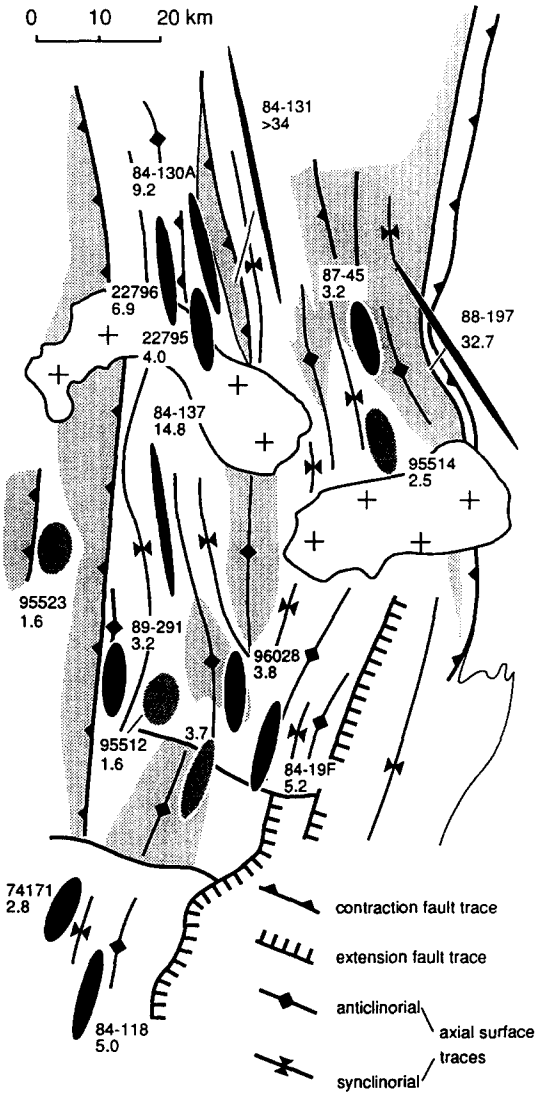

Fig. 8. Regional strain map of the eastern part of the Ballarat Slate Belt. Bulk total XZ strain ellipses projected into map view and drawn with X parallel to the cleavage traces; black ellipses: XZ strain determined from pressure shadows on pyrite, grey ellipses: XZ strain determined from graptolites. Shaded areas indicate the outcrop distribution of the Lower Ordovician (Lancefieldian stage).

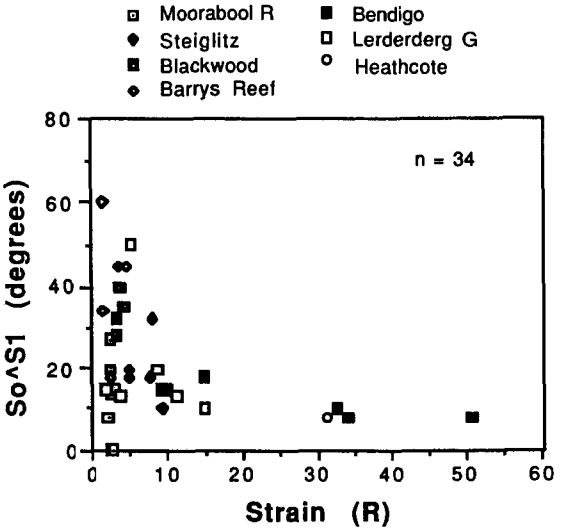

Fig. 9. Regional bulk XZ strain (R) data plotted against bedding–cleavage angle ($S_0 \wedge S_1$). The graph shows a general correlation between high bulk XZ strain ($R > 30:1$) and low bedding–cleavage angles ($S_0 \wedge S_1 < 20°$).

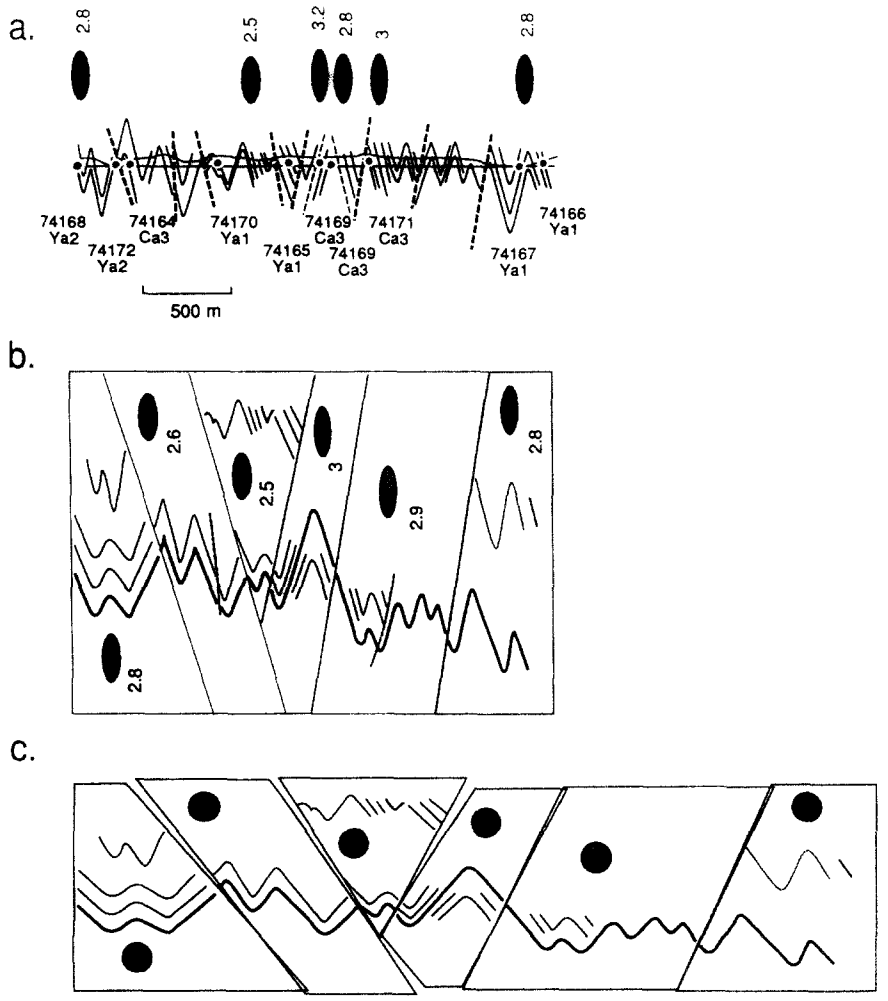

Fig. 10. Retro-deformation (unstraining) of chevron-folded and faulted sequence, Moorabool River section (see ⓒ on Fig. 2 for location) (modified from Strangward 1986). (a) Structural profile showing bedding-form lines, graptolite zonation and *XZ* strains determined from pressure shadows. (b) Restored section after removal of fault displacements showing the elements and strain data used in the retro-deformation for the flattening part of the deformation sequence. The flattening strain involves a transformation to convert the profile from (c) to (b) with a 68% vertical extension and 40% horizontal shortening. Grey ellipses are the assumed strains for elements without strain data. (c) Unstrained section using local elements as shown in (b) and assuming homogeneous strain within each element. Buckle shortening is 30%. The average fold interlimb angle in (c) is 89° (24 measurements) and is 35° (18 measurements) in (b). The heavy formline in both (b) and (c) is at the Castlemainian 3 biostratigraphic level (Ca3) and was used to calculate the respective shortenings.

Partitioning of strain within sheets

Overall shortening within individual thrusts-sheets is partitioned between chevron-folding, cleavage development in both mudstones and sandstones, and faulting (Table 1). Analysis of regional structural profiles from various parts of the thrust-belt, using simple bed-length comparison, shows that fold shortening (chevron-folding and passive limb rotation during flattening) is responsible for up to 95% of the total shortening within thrust-sheets; fold shortening ranges from 45 to 65% whereas the component due to faulting only ranges from 1 to 5% (Table 1). Structural profiles with the highest values of total shortening therefore have the smallest fold interlimb angles (Table 1).

Retro-deformation (unstraining: Hossack 1978, Cobbold 1979, Woodward *et al.* 1986) of a typical chevron-folded and faulted section from the upper part of a thrust-sheet (Fig. 10) shows that this total shortening also includes a flattening component which may be associated with cleavage development in mudstone layers (see Discussion). Unstraining was done on restored structural profiles (Fig. 10b) utilizing strains calculated from pressure shadows within mudstone layers (Fig. 10a). Retro-deformation involved coaxial unstraining of elements and their contained bedding-formlines, about the modal cleavage orientation for each element, since fibres had straight geometry in pressure shadows. The method assumes homogeneous strain distribution within mudstone layers in the selected elements (Fig. 10b) and that lithological layering behaved passively during deformation such that bedding formlines can be used to reconstruct the original geometry of the folds (Fig. 10c). Strain reversal of the section shows that chevron-fold interlimb angles change from 30–36° to 70–115° (mean: 89° from 24 measurements) after removal of the strain (compare Figs. 10b & c). Comparison of the length of section of the combined elements before and after deformation shows that shortening (e_3) due to flattening was approximately 40%.

This means that final chevron-fold shape is due to combined folding (flexural-slip chevron mechanism) and homogeneous flattening (potentially cleavage forming increments in pelites accompanied by passive limb rotation of sandstone layers) with a relative pre-flattening buckle shortening of 30% (Fig. 10c).

INCREMENTAL STRAINS AND DEFORMATION HISTORY

Upper levels of thrust-sheets

Framboidal pyrites within black to greyish black mudstones of the upper parts of thrust-sheets show straight quartz-fibres in their pressure shadows (Fig. 4c). These syn-tectonic fibrous growths are always subvertical and maintain straight morphology independent of position on folds throughout the zone. Most of the pyrites are generally small (20–50 μm in diameter) and spherical, and are located within the intercleavage domains generally enveloped by cleavage seams. Fibre lengths in pressure shadows are proportional to the size of the pyrite and the total strain (Appendix 1; cf. Beutner & Diegel 1985). Larger pyrites up to 500 μm occur and are made up of clusters of smaller subspherical pyrites. Other non-spherical types include flattened discoidal forms elongated subparallel to bedding, and euhedral pyrites which have cubic or less regular forms with distinct and planar boundaries in thin section. Euhedral types occur either in thermal aureoles and mineralized regions. There are distinct differences in fibre lengths relative to pyrite radius between framboidal and euhedral pyrites when they occur together in the one sample (see Blackwood, Appendix 1). Strains and strain histories determined from fibres adjacent to framboidal pyrites *should* reflect the total strain in the rock since they are present in the rock prior to lithification (Durney & Ramsay 1973, Ramsay & Huber 1983). However, fibres adjacent to euhedral pyrite in mineralized zones will give minimum values as there is no indication as to when the pyrites grew relative to the deformation sequence.

Fibres are generally thin interlocking needle-like crystals of quartz and white mica. They form a fringe to the pyrites and generally do not have the long tapering form characteristic of the chlorite pressure shadows in the Martinsburg Formation at Delaware Watergap (see Beutner & Diegel 1985). Tapering forms do occur in layers within slates which have transposition fabrics where the bedding is totally disrupted and segmented into an echelon ovoid fragments whose enveloping surface defines the bedding. These pressure shadows appear to consist largely of mica and reflect a marked strength contrast relative to the rock matrix.

Viewed in XZ section fibres are straight or slightly curved and essentially parallel to cleavage. In some sections (e.g. 84-118) fibres were oblique to cleavage lying between the bedding and cleavage orientation. In XY sections the fibres were also straight and as wide as the pyrites to which they were attached (i.e. there was no fibre growth parallel to Y). In YZ section no fibres were observed on pyrites, once again indicating no extension parallel to Y (i.e. $e_2 = 0$). Methods of strain determination are discussed in Appendix 2. Lack of fibre growth in Y was observed in both XY (section parallel to the cleavage plane) and XZ (section normal to the lineation defined by the fibrous overgrowths and also normal to cleavage) sections.

The straight fibres associated with the upper parts of thrust-sheets indicate a bulk coaxial deformation involving subvertical extension (e_1) of 0.3–2.9. Where measured the X direction or direction of maximum principal elongation is subvertical throughout the belt. Absence of pressure shadow growth and fibrous overgrowths in Y, the intermediate principal strain direction which lies within the cleavage suggests either a plane strain or constrictional type deformation. Lack of growth in Y indicates that there has been no subhorizontal strike-parallel extension in the thrust-belt during deformation increments related to cleavage formation in mudstone.

Determination of the three principal stretches ($1 + e_1$, $1 + e_2$, $1 + e_3$) by using either graptolites from samples with varying bedding–cleavage angles from the one outcrop (see Appendix 2), or graptolites and pressure shadows from the one sample (see Gray & Wright 1984) has enabled calculation of approximate volume changes in the upper levels of the sheets (Table 2). The deformation, where it has been analysed, is close to constant volume with volume losses <10%. These determinations agree with those of Waldron & Sandiford (1989) and Binns & Eames (1989) which question the previously published volume losses of 10–20% for Ballarat Slate Belt rocks (see the previously discussed section on *Cleavage*). The earlier calculations by Stephens *et al.* (1979) were based on comparison of cleavage (M domain) and microlithon (Q domain) chemistry and assumed that material had not been transferred into the microlithons.

Basal part of thrust-sheets

Curved fibrous growths of quartz occur in pressure shadows on pyrite within the basal parts of thrust-sheets in the Ballarat Slate Belt (Figs. 4d and 5a). Strongly lineated mudrock in the hanging walls of the Muckle-

Table 2. Volume change and principal stretches determined from pelites in the Ballarat Slate Belt

Location	$1 + e_1$	$1 + e_2$	$1 + e_3$	ΔV
Ingliston*	1.8	1.0	0.5	−8.5%
Ingliston*	1.8	1.1	0.5	0.65%
Steiglitz†	3.0	1.0	0.29	−13%
Steiglitz†	3.0	1.0	0.3	−10%

*Based on graptolite data from Hills & Thomas (1944). Their data shows $1 + e_2$ ranges between 1 and 1.2.

†Based on graptolites in bedding ($1 + e$), $S_0 \wedge S_1 \approx 25°$, and a maximum principal stretch ($1 + e_1$) determined from pressure shadows in the same handspecimen that contained the graptolites (see Ramsay & Huber 1983, p. 91).

ford, Whitelaw and Heathcote faults (Fig. 7) show pressure shadows with long tapering tails made up of curved bladed crystals of quartz. The tips of the pressure shadows tend to taper and curve in opposite directions giving aggregates a sigmoidal appearance. Pressure shadows from all the samples investigated have similar shape and the same curvature (looking north parallel to the cleavage–bedding intersection lineation; Fig. 7) and indicate non-coaxial deformation during growth of the pressure shadows. In sections cut parallel to the cleavage (approximating XY sections) pressure shadows show vertically oriented, blade-like quartz crystals with no fibre growth parallel to Y; some pressure shadows do show slight curvature in a clockwise growth sense in XY, but generally have straight fibrous form.

Many of the long curved fibres display sweeping extinction, particularly in their outermost segments towards the extremities of the pressure shadows (Fig. 5a). Marked subgrain and new grain growth also occurs in these regions (Fig. 4e). Individual fibres have smooth to undulating boundaries (Fig. 5b), with undulating forms associated with bleb-like subgrain development. Individual bulges along fibre boundaries have boundary-orthogonal cracks which are coincident with the thinnest parts of the fibres (Fig. 5d). Undulose extinction and development of subgrains and new grains in many pressure shadows indicates that much of the quartz has been deformed either during or subsequent to growth (Fig. 5e). Also, the ends of many of the pressure shadows terminate against and are truncated by dark cleavage seams or folia (Figs. 4d and 7c).

Towards the pyrite, partition lines separate different fibre orientations and morphologies (Fig. 5b), demarcating different growth stages within the pressure shadows. Fibres in contact with the pyrite are composed of thinner and more fibrous quartz, whereas fibres in the outermost parts of pressure shadows have wide bladed forms and show the most effects of deformation (Fig. 5a). These fibres also abut and are truncated by cleavage seams. In many instances the outer parts of pressure shadows are missing due to removal by pressure solution (dissolution). That deformation of the outermost fibres is most intense and that they show truncation against cleavage seams suggests these fibres are older, and therefore that the quartz-pressure shadows, like others documented in slates, display antitaxial growth. This means growth sense towards the host with new fibre growth at the interface with the opaque material.

Problems with recrystallization of the fibres, particularly in the most external parts of the shadows, and the dissolution and removal of the early fibres, as indicated by the truncation of the pressure shadows against dark cleavage seams (see insets 88-197A, B and C, Fig. 11b) can be assessed on these graphs. Individual pyrites from the same rock volume, given homogeneous strain which appears a reasonable assumption at the scale of a thin section in these rocks, should show similar incremental extension histories and therefore similar step functions/histograms. Missing fibre segments cause displacement of step histograms which can be easily detected if sufficient pyrites are measured, particularly those without noticeable truncations by cleavage seams.

As the fibres are recrystallized in their outer segments, analysis of incremental strains for the basal parts of these thrust-sheets is problematic. Fibre curvature from both localities indicates a clockwise rotation of the shadow with respect to the pyrite during growth of the pressure shadow. This is in agreement with the rotation expected for simple shear deformation at the base of thrust-sheets (Elliott 1976, Wojtal 1986). Either relict partition lines between impinging fibres of differing orientations and ghost-fibre inclusion trails (Figs. 5a, b & d; Whitelaw fault), or the boundaries of relict, bladed quartz-fibres within the shadows (Figs. 4d & e; Heathcote fault) were used to calculate the totals strains and incremental strain history for these hanging wall positions (see Appendix 2). This gave XZ strains greater than 30:1 for both the Whitelaw and Heathcote fault hanging walls. Relative rates of rotation vs incremental elongation (e_1) based on this approximation (Fig. 11) show similar but not identical, deformation sequences for the hanging walls of the Whitelaw and Heathcote faults, respectively. Both show moderate degrees of non-coaxiality with increments fluctuating over a range of approximately 40°. The simplest deformation sequence is recorded by the Whitelaw fault pressure shadows which show a continuous and progressive clockwise rotation. The slopes of the envelope of these cumulative incremental extension graphs (Fig. 11a) are less than that expected for simple shear and matches the accumulations of total strain for sequences between progressive pure shear and progressive simple shear (i.e. $0 < \omega_i < 5.45°$; Ramsay & Huber 1983, p. 229). Pressure shadows from the hanging wall of the Heathcote fault show fluctuating rotations over 45°, with early flattish segments on the graphs ($\Sigma e_1 < 1.2$, Fig. 11b) indicating high elongations with low rates of rotation typical of non-ideal simple shear deformation (Gray & Durney 1979, Ramsay & Huber 1983). Latest increments ($\Sigma e_1 > 1.2$, Fig. 11b) approach that expected for progressive simple shear, which is characterized by a constant slope of one radian per strain unit ($\delta\phi/\mathrm{de1} = 5.7°/0.1$; step graph A on Figs. 11a & b) and an increment orientation which remains at 45° to the shear axis (see Gray & Durney 1979, p. 72).

When compared to the upper portions of thrust sheets, rocks adjacent to the major strike-parallel faults have clearly undergone a different deformational history involving significantly higher strains and a marked rotational component to the deformation.

DISCUSSION

The geometry of folds within nappes and thrust-sheets provides insight into the mechanics of thrust-sheet emplacement (e.g. Sanderson 1979, Ramsay *et al.* 1983, Gibson & Gray 1985, Ridley & Casey 1989). Many thrust-sheets are shortened in the transport direction (e.g. case $\alpha < 1$, where α is the stretch in the shear

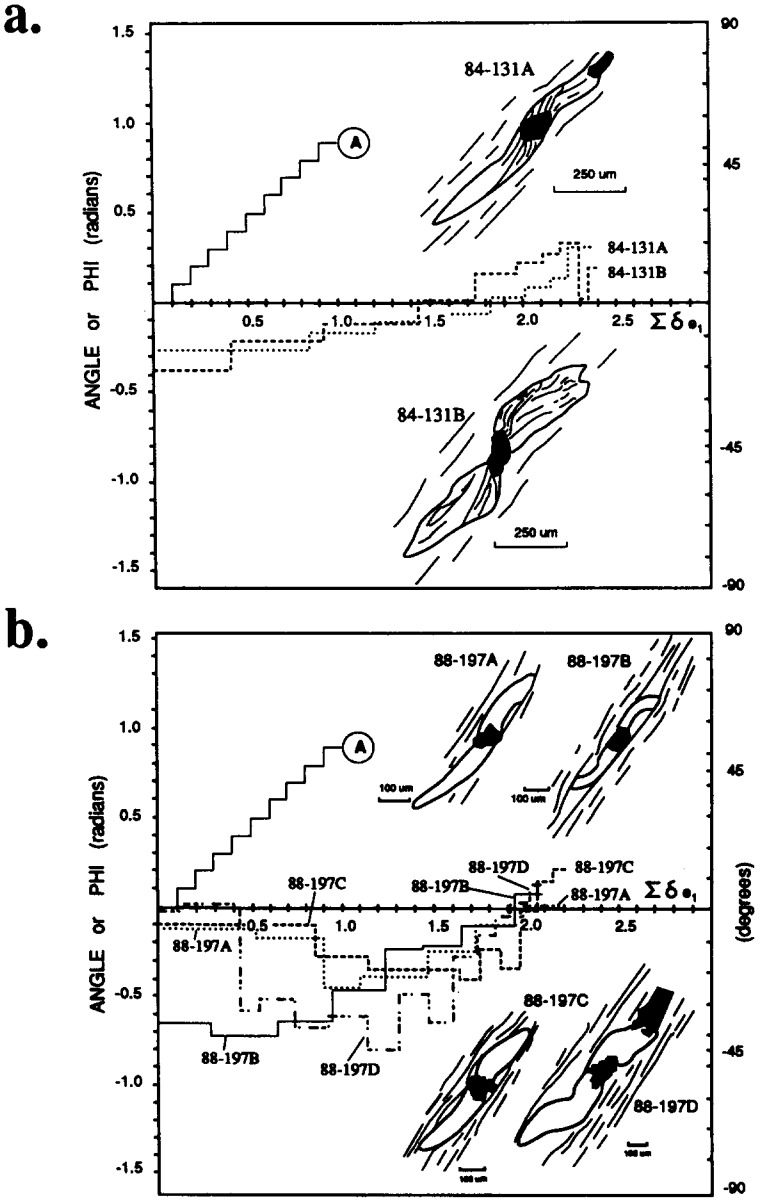

Fig. 11. Incremental extension graphs showing the magnitude of extension increments (δe_1) relative to angular changes in the incremental extension direction (angle/phi) during the deformation period recorded by the pressure shadows for (a) the Whitelaw fault and (b) the Heathcote fault. Insets are sketches of the pressure shadows analysed. Step graphs labelled A are those for progressive simple dextral shear. Note the offset in the steps of the cumulative incremental extension graph for 88-197B compared to the step-graphs for other pressure shadows in the same thin section. This indicates that the early increments are missing, and removed by dissolution as shown by truncation of the pressure-shadow along the bounding cleavage traces (see inset sketch).

direction; Sanderson 1982, fig. 6) and show internally heterogeneous shear strains varying with depth above their basal detachments. Folds, faults and cleavage in most cases can be related to ductile shearing strain which diminishes to zero towards the upper parts of thrust-sheets (Elliott 1976, Mitra & Elliott 1980). At shallow crustal levels deformation within thrust-sheets occurs by passage of the sheets through alternating regimes of extending and compressing flow (e.g. Elliott 1977). Thickening and shortening of their upper parts has been attributed to the cyclical passage of a zone of compressive flow through the moving thrust-sheet during emplacement. Movement of material in the sheet into the compressive zone occurs at a faster rate than it can leave. Such behaviour, common in glaciers and ice sheets (Hudleston & Hooke 1980), is shown by overprinting arrays of minor faults where inhomogeneous deformation is due to displacement of blocks on discrete, mineral-coated surfaces (e.g. Wojtal 1986, Woodward *et al.* 1988).

Documented strain gradients within thrust-sheets range from a variation in XZ strains between 1.5:1 and 5:1 up to 5 m from the basal detachments of Appalachian Valley and Ridge sheets (Wojtal 1986), shear strain (γ) variations from <3 on the upper limb to 8–10 on the lower limb of the Morcle nappe of the Swiss Helvetic zone (Ramsay *et al.* 1983), shear strain (γ) variations from >3 on the lower limb to approximately

uniform values <1 in the upper limb of thrust nappes in (Sanderson 1979), and shear strain (γ) variations from approximately uniform values <5 in the upper parts of thrust-sheets to $\gamma > 15$ up to 500 m above thrusts in the Finnish Caledonides occur (see Coward & Kim 1981). For the thrust-sheets in eastern Australia shear strain varies from $\gamma = 0$ in the upper parts to $\gamma > 8$ in their basal zones, and there is a more uniform shortening (>60%; i.e. beyond that for chevron-fold lock-up) throughout individual thrust-sheets. This shortening occurs prior to final thrusting, because detachment faults which splay or cut up-section clearly truncate chevron-folds in both the footwall and hanging wall. This internal deformation must be essential to sliding on the basal detachment.

Implications of fibre patterns and strains

That (1) fibres in pressure shadows in the upper parts of thrust-sheets are always straight and subvertical independent of their position on folds, and (2) retro-deformation of folded profiles by removal of strain estimates, as determined from these pressure shadows, produces fold profiles whose limb angles are range between 70° and 115°, requires post-buckling development of cleavage. Strain accumulation in pelites as recorded by syn-tectonic fibre growth in pressure-shadows, and presumably cleavage development as well, appears to have been suppressed until limb dips of approximately 45° had been achieved. The extensive development of bedded veins, requiring significant interlayer-slip, suggests that initial thrust-sheet shortening was purely by flexural-slip folding. Straight fibres require coaxial deformation increments and suggest that cleavage is a consequence of fold-flattening. This flattening also caused about 35–40% shortening of thrust-sheets in the inferred tectonic-transport direction, tightening of chevron-folds beyond lock-up angles by passive limb-rotation, and overall thickening of thrust-sheets. Weak regional fanning of cleavage supports this contention, as fanning would require partitioning of shear strain to the mudstone layers and therefore a component of flexural flow during chevron-fold development.

Approximately simultaneous increments of flattening and buckling to achieve the final fold shapes (Huddleston 1973) should produce curved fibres in pressure shadows along fold limbs (Beutner & Diegel 1985). These are clearly not observed. Straight fibres could only be produced in this situation when limb rotation (spin rotation component) precisely balanced within-layer shear-induced rotations (vorticity rotation component) (Lister & Williams 1983). Maintenance of this situation everywhere throughout deforming thrust-sheets with volumes on the order of 10^4 km^3 is highly unlikely.

Fibre patterns indicate that hanging wall rocks adjacent to faults have undergone a totally different incremental strain history to rocks more distant from these faults. There are no early straight segments to match the interpreted subvertical elongations experienced by rocks outside these zones. Fibres indicate that the more intense cleavage development and very low bedding–cleavage angles (<20°) in zones influenced by developing faults (see Fig. 7) is due to a non-coaxial deformation sequence. The varying intensity of the cleavage and continuous curvature of the patterns of syntectonic crystal fibres suggests that the observed features are part of the same progressive and continuous deformation. Rocks adjacent to developing fault zones were therefore undergoing a strong rotational deformation, whereas at approximately the same time rocks away from faults were undergoing a plane strain coaxial deformation involving horizontal shortening and vertical extension.

Folding mechanisms

The nature of the layers and an approximately constant ratio of competent to incompetent layer thickness requires a chevron style of folding (Ramsay 1974). Where anomalously thick or thin competent layers occur, the formation of limb thrusts, bulbous hinge zones, ductile flow parallel to bedding, hinge collapse structures and hinge dilation structures will accommodate geometric problems. Theoretical considerations predict that chevron folds lock-up at an interlimb angle approaching 60° (De Sitter 1958), although the exact angle is a function of the frictional properties between layers (Ramsay 1974). In the Ballarat Slate Belt, frictional resistance presumably overcame layer-parallel slip at fold lock-up, with subsequent shortening due to fold-flattening. This occurred largely by cleavage development in the intervening pelites and the development of hinge accommodation structures which in turn nucleated some strike faults.

A flexural folding mechanism is responsible for chevron-fold development. Fibrous shear veins transitional into bedded veins and laminated veins (Chace 1949, Cox 1987, Willman *et al.* in preparation) indicate inter-bed slippage approximately orthogonal to fold hinges. Limb dips of approximately 50–65° (assuming a reasonable range of fold interlimb angles from 30° to 50°; Table 1) require fold-limb interbed shear strains (γ) of 0.9–1.1, where the angular shear (ψ) varies from 41° to 48° (see Ramsay 1967, fig. 7.57). Retro-deformation (see Strain Partioning section) has enabled calculation of 'buckling' and 'pure shear' limb-rotation components (cf. Shimamoto & ·Hara 1976, Odling 1987) for the chevron-folds. Assuming the layers were initially horizontal, then the 'buckling' component of limb rotation is approximately 45° and the 'pure shear' (fold flattening) component is 15°.

Cleavage development in pelites is therefore considered largely due to shortening and thickening of thrust-sheets *after* chevron-folds had attained limb dips of approximately 45°. The low XZ strains on fold limbs in sandstone layers (Appendix 1) probably reflects an early layer-parallel shortening strain, whereas the increased values in the vicinity of fold hinges ($\approx$1.7) is due to flattening after fold lock-up.

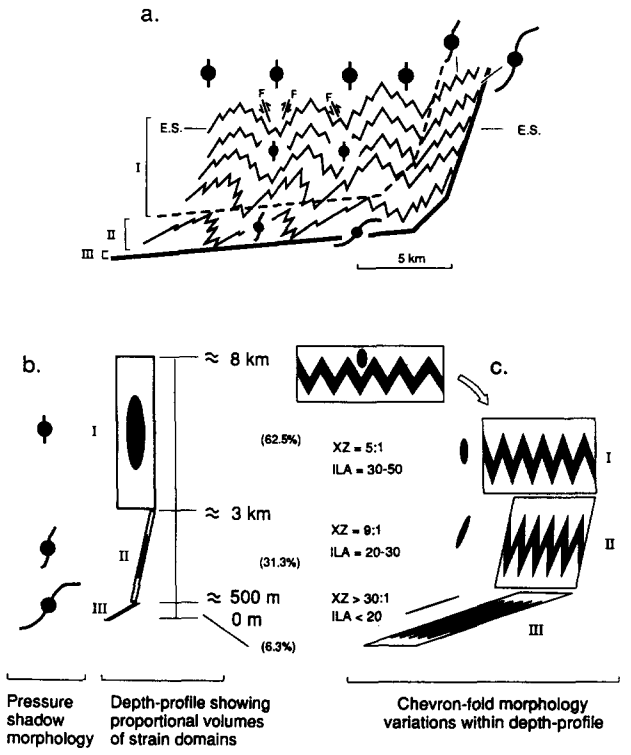

Fig. 12. Overall geometry and strain profile of a typical Ballarat Slate Belt chevron-folded thrust-sheet (based largely on observations from within the Whitelaw thrust-sheet). (a) Schematic diagram showing the inferred changes in fold-geometry with depth and the variations in the length and curvature of quartz-fibres in pressure shadows through the sheet. Axial surfaces of regional anticlinoria and synclinoria, as well as cleavage traces, should flatten with depth to become asymptotic to the basal thrust. (b) Vertical strain profile within a thrust-sheet where domains I, II and III reflect differences in XZ strain magnitude, fold tightness and shear strain (γ) magnitude. Percentages in brackets are an expression of the relative thickness of each strain domain with respect to the total thrust-sheet thickness. (c) Typical fold geometries within the strain domains I, II and III; ILA is the fold interlimb angle (degrees).

Thrust-sheet deformation model

Elements such as fold shape and syntectonic-fibre geometries in pressure shadows contained within Ballarat Slate Belt thrust-sheets, combined with knowledge of fault-attitude variations with depth (Gray *et al.* in press), have enabled extrapolation of these data to develop a generalized model of thrust-sheet geometry (Fig. 12). The model presented is based on deformational effects preserved in the present approximately planar erosion surface (ES in Figs. 3a and 12a). The model geometry incorporates a gently dipping regional-fold enveloping surface, listric fault-shape with depth, a marked gradient in strain (Fig. 12b) and a change in chevron-fold geometry (Fig. 12c) from the top to bottom of individual thrust-sheets. A consequence of this model is that development of the décollement between cover (Ordovician sequence) and basement (Cambrian) and the propagation of listric faults at depth is considered coeval with the formation of folds and cleavage at higher structural levels within individual thrust-sheets. Contraction along layers subparallel to the shear surfaces produced upright buckle folds which were later modified to tight, inclined folds by localized non-coaxial deformation (up to 3 km from faults) associated with development of major faults (Fig. 12c).

Internal sheet deformation, initially governed by sliding along bedding surfaces to produce chevron folds, is a consequence of basal sliding to maintain continuity of the thrust-sheet during displacement on the basal fault. Chevron-folding largely pre-dates the final phase of thrusting which caused emplacement of thrust-sheets to their present levels in the crust; chevron folded sequences are truncated by thrust faults. This is in contrast to North American foreland thrust-sheets where folding, largely synchronous with sheet emplacement, is a consequence of irregularities in the underlying thrust-surface. Continued shortening required (1) development and upward propagation of splay faults off the main detachment, and (2) emplacement of lower parts of the stratigraphy to shallower crustal levels along these splays accompanied by internal thrust-sheet deformation. Internal deformation was by cleavage development, tightening of chevron-folds and minor faulting.

Observed gradients in strain within the Ballarat Slate Belt appear related to faults; highest strains occur in hanging walls immediately adjacent to fault traces (Fig. 6). A zonation of thrust-sheets into upper and lower parts (based on the geometry of chevron-folds, the intensity of cleavage, the magnitude of XZ strain, and the type of incremental strain history) reflects a variation in the deformation history through individual sheets during thrust-sheet emplacement (Figs. 12b & c). A coaxial, plane strain, approximately constant volume deformation characterizes the upper parts of thrust-sheets (i.e. $\gamma \approx 0$), whereas the basal 3 km reflect a non-coaxial high strain deformation involving shear strains (γ) in excess of 5 (i.e. $\psi > 78°$, where ψ is the angular shear). Fibre-growth patterns in pressure shadows indicate (1) no evidence of extension normal to the inferred transport direction (i.e. parallel to fault map traces) within sheets (i.e. a plane strain deformation), (2) no evidence of wrenching or transpressional deformation within individual thrust-sheets, and (3) no complexities in fibre geometry relatable to passage of thrust-sheets over ramps and/or irregularities in the basal detachment.

Controls on internal deformation of thrust-sheets

The relative strengths of décollement horizons (basal detachments) and individual thrust-blocks control the mechanics of thrust-sheet emplacement (Schmid 1975) and the amount of internal deformation within thrust-sheets (Elliott 1976). Where a sheet is moving on a weak horizon (flow stress < 100 bars), little internal deformation will accompany thrust-sheet emplacement (e.g. Schmid 1975, Gilotti & Kumpulainen 1986). In contrast, where the yield stress of the décollement zone is similar to that of the thrust-block, significant internal deformation (e.g. folding and cleavage development) should accompany sheet emplacement.

Lithological similarity (interbedded sandstone and mudstone) accompanied by approximately similar pro-

portions of sand-to-shale throughout the quartz-rich turbidite succession of the Ballarat Slate Belt means that there is no lithologically-controlled décollement horizon as has been observed in other thrust belts (e.g. Glarus calc-mylonite in the Helvetic alps: Schmid 1975; Rome shales in the southern Appalachian thrust-belt: Harris & Milici 1977). Detachment in the sequence occurs within the lowermost Ordovician (Lancefieldian biostratigraphic stage) with thick, massive, amalgamated sandstones predominantly occurring in the hanging walls of major faults. That the basal parts of these turbidite-dominated thrust-sheets do show higher strains, intense phyllitic cleavage, lower chevron-fold interlimb angles (>30°), and very low bedding–cleavage angles (>10°) suggests that strain softening within the basal zones has controlled their emplacement.

Effects upon thrust-sheets due to movement on ramps

Faults may be simplified into a sub-horizontal basal detachment (flat) and a steeper segment (ramp) where they cut up stratigraphic section (see Fig. 12). Emplacement of a thrust-sheet to a higher crustal level requires bending of the sheet due to leading-edge-up shear as it passes through the closing bend at the base of the ramp (e.g. Sanderson 1982). Does this ramp-induced shear strain cause change in chevron-fold geometry and the overall strain history of the thrust-sheets?

Discrepancy between shear strains in the basal zones of thrust-sheets and their observed displacement indicates that for certain thrust-faults the high basal strains must relate to their initiation as major sub-horizontal shear zones rather than to their total translation history (e.g. Boullier & Quenardel 1981, Milton & Williams 1981). Multiple cleavages within thrust-sheets and changes in the fibre geometry of the pressure shadows have also been related to passage of thrust-sheets through closing bends (cf. Sanderson 1982, Beutner *et al.* 1988). These features are not observed in the Ballarat Slate Belt. Multiple cleavages only occur adjacent to faults and are not common within individual sheets (Gray & Willman 1991). Also, changes in fibre geometry do not match those expected for the kinematics of deformation at a thrust-fault ramp (cf. Beutner *et al.* 1986).

The question remains as to whether changes in strain state and chevron-fold geometry are part of a *continuous* deformation sequence which has been affected by passage from flat to ramp. Transport of a layer up a ramp involves rotation of the layer as it moves from the flat to the ramp segment. This rotation would cause chevron-fold axial surfaces to dip toward the fault-ramp, rather than steeply away from it as is observed (Fig. 6); such a change can be observed by simply flexing a sheet of foam which has been inscribed with chevron-folds. Leading-edge-up high shear strains are needed on the ramp to produce chevrons with axial surfaces which dip to the west (i.e. away from the ramp). This is demonstrated by modelling of deformation sequences by factorization of strains into homogeneous components of pure shear, rigid-body rotation and simple shear components (Fig. 13). For each of the three different deformation sequences illustrated the chevrons become markedly asymmetric, tight and inclined; interlimb angle from 65° (I), to 20° (II and III), to 15° (IV). Chevrons with W-dipping axial surfaces (i.e. axial surfaces dipping away from the fault-ramp) require a significant component of simple shear on the ramp (Fig. 13b), which implies continued deformation within the basal zone with passage of the folded sequence from flat to ramp. Flattening due to compressive flow in the toes of the thrust-sheets cannot produce chevrons with W-dipping axial surfaces, either with an early simple shear component on the flat (Fig. 13c) or a late simple shear component on the ramp (Fig. 13d).

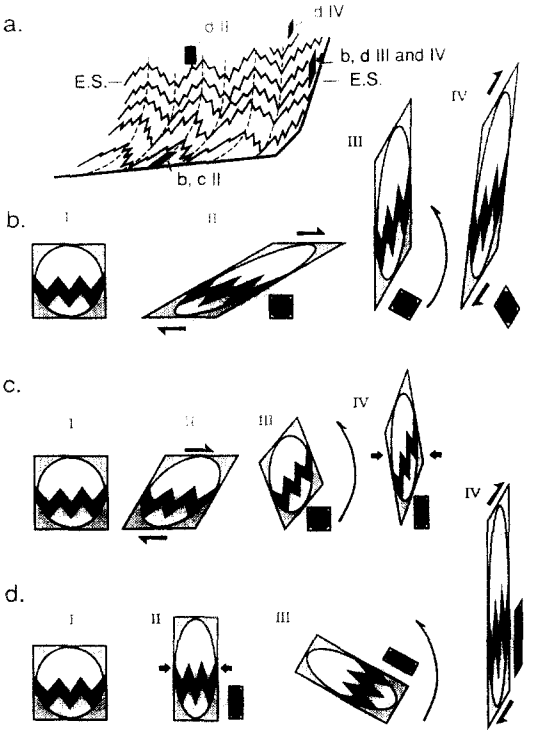

Fig. 13. Schematic deformation sequences with factorisation of strain into homogeneous components of pure shear, simple shear and rotation. In each case stage I is the initial state (with chevron-fold interlimb angles of 65°), stage II involves deformation along the lower hanging wall flat, III involves rigid-body rotation of the sheet from the lower flat onto the ramp, and IV involves deformation of the hanging wall on the ramp. (a) Schematic diagram of a typical Ballarat Slate Belt thrust-sheet showing the postulated positions of the various strain states for the strain histories in (b)–(d). The lower case characters refer to the particular deformation sequence whereas the roman numerals refer to the particular strain state within the overall strain history. (b) Deformation sequence involving II simple shear ($\psi = 60°$, where ψ is the angular shear), III rotation (60°) and IV simple shear ($\psi = 30°$). (c) Deformation sequence involving II simple shear ($\psi = 30°$), III rotation (60°) and IV pure shear (2.3:1). (d) Deformation sequence involving II pure shear (2.3:1), III rotation (60°) and IV simple shear ($\psi = 60°$).

Mechanics of thrust-sheet emplacement

Thrust-sheet emplacement involves either spreading or gliding behaviour of the sheet induced by gravitational collapse or externally applied forces (Elliott 1976, Chapple 1978, Merle 1986). That the upper parts of Ballarat thrust-sheets have undergone shortening and

show marked strain gradients towards their basal zones (Fig. 12) suggests that sheets have behaved as strong plastic wedges which shortened and thickened by compressive flow in their upper parts accompanied by sliding along a strain-softened weak basal zone. This weak zone constitutes the lower 2–3 km of sheets with marked effects in the basal 500 m. Sheet emplacement was essentially by ductile flow confined to a thin strain-softened high strain layer. Such behaviour is best modelled by viscous gliding along a low viscosity basal zone but with ductile yield throughout all parts of the overlying thrust-sheet. The presence of steep foliation and the documented horizontal shortening for the thrust-sheets of the Ballarat Slate Belt (i.e. the case where $\alpha < 1$, Sanderson 1982) indicate that gravitationally induced spreading has not been important during emplacement (cf. Merle 1986, fig. 8). Thus a push from the rear involving underthrusting and crustal stacking is required as a driving force (Gray *et al.* in press).

CONCLUSIONS

(1) Chevron folds, high angle reverse faults and spaced cleavage characterize crustal shortening above subsurface detachment faults in a monotonous quartz-rich turbidite succession of interbedded mudstones and sandstones.

(2) High-angle reverse faults at the surface have listric form and flatten with depth to join detachment faults with occur at the base of the Ordovician turbidite succession and within the underlying Cambrian metavolcanics and volcaniclastic sequence.

(3) Strain domains exist within thrust-sheets; a low strain zone (domain I) characterized by coaxial deformation in the upper parts of thrust-sheets and higher strain domains (II and III) involving non-coaxial deformation in the lower parts of sheets (Fig. 12).

(4) Approximately constant volume, plane strain coaxial deformation of the upper parts of thrust-sheets produced upright, close chevron-folds, spaced cleavage and both E- and W-dipping minor contraction faults (domain I).

(5) Cleavage development in pelites occurred during shortening and thickening of thrust-sheets *after* chevron fold-lock up (i.e. during fold flattening).

(6) Intense phyllitic cleavage, strong down-dip stretching lineations, decreased chevron-fold interlimb angles and changes in axial surface dip are products of a non-coaxial high strain deformation in the basal 3 km of thrust-sheets (domains II and III).

(7) Pressure shadows on pyrite suggest incremental rotations (ω_i) between those expected for pure shear and simple shear (i.e. $0 < \omega_i < 5.45°$), implying that deformation in the basal zone was non-ideal simple shear (domain III).

(8) Thrust-sheets dominated by turbidite sequences have been emplaced on strain-softened basal zones dominated by asymmetric folds and intense cleavage. That stretch (α) values are <1 and within-sheet extensions are subvertical indicates their emplacement did not involve gravitationally induced spreading, but required a push from the rear during collisional orogenesis.

Acknowledgements—The research was supported by Australian Research Council Grant E8315675 (awarded to D. R. Gray) and Monash University Special Research Funds. Part of the work at Bendigo and Chewton-Castlemain was done by C. E. Willman as part requirement for an M.Sc. degree. We thank Stephen Cox and Ed Beutner for constructive reviews, Colleen Elliott for comments, and Sons of Gwalia N.L. for releasing the Heathcote drill core sample containing the pressure shadows and allowing publication of the drill-hole data. D. R. Gray acknowledges use of facilities in the Geology Department at the University of Otago, Dunedin, New Zealand, where the final paper preparation was undertaken.

REFERENCES

Beutner, E. C. & Diegel, F. A. 1985. Determination of fold kinematics from syntectonic fibers in pressure shadows, Martinsburg Slate, New Jersey. *Am. J. Sci.* **285**, 16–50.

Beutner, E. C., Fisher, D. M. & Kirkpatrick, J. L. 1988. Kinematics of deformation at a thrust fault ramp (?) from syntectonic fibers in pressure shadows. *Spec. Pap. geol. Soc. Am.* **222**, 77–88.

Binns, R. A. & Eames, J. C. 1989. Geochemistry of wall rocks at the Clunes gold deposit, Victoria. *Econ. Geol. Monogr.* **6**, 310–319.

Boullier, A.-M. & Quenardel, J.-M. 1981. The Caledonides of northern Norway: relation between preferred orientation of quartz lattice, strain and translation of nappes. In: *Thrust and Nappe Tectonics* (Edited by Coward, M. P. & McClay, K. R.). *Spec. Publs geol. Soc. Lond.* **1**, 185–195.

Brun, J. P. & Merle, O. 1985. Strain patterns in models of spreading-gliding nappes. *Tectonics* **4**, 705–719.

Cas, R. A. F. & VandenBerg, A. H. M. 1988. Ordovician, In: *Geology of Victoria* (2nd edn) (edited by Douglas, J. G. & Ferguson, J. A.). *Victn Div. geol. Soc. Aust.*, 63–102.

Chace, F. M. 1949. Origin of the Bendigo saddle reefs with comments on the formation of ribbon quartz. *Econ. Geol.* **44**, 561–597.

Chappell, B. W., White, A. J. R. & Hine, R. 1988. Granite provinces and basement terranes in the Lachlan fold belt, southeastern Australia. *Aust. J. Earth Sci.* **35**, 505–524.

Chapple, W. M. 1978. Mechanics of thin-skinned fold- and thrust-belts. *Bull. geol. Soc. Am.* **89**, 1189–1198.

Cobbold, P. R. 1979. Removal of finite deformation using strain trajectories. *J. Struct. Geol.* **1**, 67–72.

Coward, M. P. & Kim, J. H. 1981. Strain within thrust-sheets. In: *Thrust and Nappe Tectonics* (edited by Coward, M. P. & McClay, K. R.). *Spec. Publs geol. Soc. Lond.* **1**, 275–292.

Cox, S. F. 1987. Antitaxial crack-seal vein microstructures and their relationship to displacement paths. *J. Struct. Geol.* **9**, 779–787.

Cox, S. F., Ceplecha, J., Wall, V. J., Etheridge, M. A., Cas, F. A. F., Hammond, R. & Willman, C. 1983. Lower Ordovician Bendigo Trough sequence, Castlemaine area, Victoria—deformation and implications for the tectonic evolution of the Lachlan Fold belt. *Geol. Soc. Aust. Abs.* **9**, 41–42.

Crawford, A. J. & Keays, R. R. 1978, Cambrian greenstone belts in Victoria; marginal sea-crust slices in the Lachlan foldbelt of southeastern Australia. *Earth Planet. Sci. Lett.* **41**, 197–208.

De Sitter, L. U. 1958. Boudins and parasitic folds in relation to cleavage and folding. *Geologie Mijnb.* **17**, 1–11.

Durney, D. W. & Ramsay, J. G. 1973. Incremental strains measured by syntectonic crystal growths. In: *Gravity and Tectonics* (edited by De Jong, K. A. & Scholten, R.). Wiley, New York, 67–96.

Elliott, D. 1976. The energy balance and deformation mechanisms of thrust-sheets. *Phil. Trans. R. Soc. Lond.* **A283**, 289–312.

Elliott, D. 1977. Some aspects of the geometry and mechanics of thrust belts. Part II. Unpublished Notes, 8th Annual C.S.P.G. Seminar, Calgary.

Etchecopar, A. & Malavielle, J. 1987. Computer models of pressure shadows: a method for strain measurement and shear-sense determination. *J. Struct. Geol.* **9**, 667–677.

Fergusson, C. L., Gray, D. R. & Cas, R. A. F., 1986. Overthrust terranes in the Lachlan fold belt, southeastern Australia. *Geology* **14**, 519–522.

Fisher, M. & Coward, M. 1982. Strains and folds within thrust-sheets:

an analysis of the Heilam sheet, northwest Scotland. *Tectonophysics* **88**, 291–312.
Fry, N. 1979. Random point distributions and strain measurements in rocks. *Tectonophysics* **60**, 89–105.
Geiser, P. A. 1988. Mechanisms of thrust propagation: some examples and implications for the analysis of overthrust terranes. *J. Struct. Geol.* **10**, 829–845.
Gibson, R. G. & Gray, D. R. 1985. Ductile-to-brittle transition in shear during thrust-sheet emplacement, southern Appalachian thrust belt. *J. Struct. Geol.* **7**, 513–525.
Gilotti, J. A. & Kumpulainen, R. 1986. Ductile flow in the Sårv thrust-sheet, Scandinavian Caledonides. *J. Struct. Geol.* **8**, 441–455.
Glasson, M. J. & Keays, R. R. 1978. Gold mobilisation during cleavage development in sedimentary rocks from the Auriferous slate belt of central Victoria, Australia: some important boundary conditions. *Econ. Geol.* **73**, 496–511.
Gray, D. R. 1988. Structure and Tectonics. In: *Geology of Victoria* (2nd edn) (edited by Douglas, J. G. & Ferguson, J. A.). *Victn Div. geol. Soc. Aust.*, 1–36.
Gray, D. R. & Durney, D. W. 1979. Investigations on the mechanical significance of crenulation cleavage. *Tectonophysics* **58**, 35–79.
Gray, D. R. & Willman, C. E. 1985. Structural relations in central Victoria and implications for crustal structure. *Abs. Victorian Lithosphere Symposium*, Melbourne University, Melbourne, 19–21.
Gray, D. R. & Willman, C. E. 1991. Deformation in the Ballarat Slate belt, central Victoria and implications for crustal structure across SE Australia. *Aust. J. Earth Sci.* **38**, 171–201.
Gray, D. R., Wilson, C. J. L. & Barton, T. J. In press. Intracrustal detachments and crustal evolution within the Lachlan Fold belt, southeastern Australia. *Geology*.
Gray, D. R. & Wright, T. O. 1984. Problem of volume loss, fabric development and strain determination in low grade pelitic rocks: Martinsburg Formation, U.S.A. (Abst. Bermagui Conf. 1984). *J. Struct. Geol.* **7**, 492.
Harris, L. D. & Milici, R. C. 1977. Characteristics of thin-skinned style of deformation in the southern Appalachians and potential hydrocarbon traps. *Prof. Pap. U.S. geol. Surv.* **1018**.
Harris, W. J. & Thomas, D. E. 1938. A revised classification and correlation of the Ordovician graptolite zones of Victoria. *Min. geol. J. Vict.* **1**, 62–72.
Hills, E. S. & Thomas, D. E. 1944. Deformation of graptolites. *Geol. Mag.* **81**, 216–222.
Hills, E. S. & Thomas, D. E. 1954. Turbidity currents and the graptolite facies. *J. geol. Soc. Aust.* **1**, 119–133.
Hossack, J. R. 1978. The correction of stratigraphic sections for tectonic finite strains in the Bygdin area, Norway. *J. geol. Soc. Lond.* **135**, 229–241.
Hudleston, P. J. 1973. An analysis of 'single layer' folds developed in a viscous media. *Tectonophysics* **16**, 189–214.
Hudleston, P. J. & Hooke, R. LeB. 1980. Cumulative deformation in the Barnes ice cap and implications for the development of foliation. *Tectonophysics* **66**, 127–146.
Kirchner, I. 1987. Structural controls on gold mineralisation of the Blackwood region. Unpublished B.Sc. (Hons.) thesis, Monash University, Melbourne, Australia.
Odling, N. 1987. The determination of 'buckling rotation' and its application to theoretical and experimental models of buckle folds. *J. Struct. Geol.* **9**, 1021–1028.
Lister, G. S. & Williams, P. F. 1983. The partitioning of deformation in flowing rock masses. *Tectonophysics* **92**, 1–33.
Merle, O. 1986. Patterns of stretch trajectories and strain rates within spreading-gliding nappes. *Tectonophysics* **124**, 211–222.
Milton, N. J. & Williams, G. D. 1981. The strain profile above a major thrust fault, Finnmark, N. Norway. In: *Thrust and Nappe Tectonics* (Edited by Coward, M. P. & McClay, K. R.). *Spec. Publs geol. Soc. Lond.* **1**, 235–239.
Mitra, G. 1984. Brittle to ductile transition due to large strains along the White Rock thrust, Wind River Mountains, Wyoming. *J. Struct. Geol.* **6**, 51–61.
Mitra, G. & Elliott, D. 1980. Deformation of basement in the Blue Ridge and the development of South Mountain cleavage. In: *The Caledonides of the U.S.A.* (edited by Wones, D. R.). *Dept Geol. Sci., Virgina Tech. Mem.* **2**, 307–311.
Ramsay, J. G. 1967. *Folding and Fracturing of Rocks*. McGraw-Hill, New York.
Ramsay, J. G. 1974. Development of chevron folds. *Bull. geol. Soc. Am.* **85**, 1741–1754.
Ramsay, J. G., Casey, M. & Kligfield, R. 1983. Role of shear in the development of the Helvetic fold-thrust belt of Switzerland. *Geology* **11**, 439–442.
Ramsay, J. G. & Huber, M. I. 1983. *The Techniques of Modern Structural Geology, Volume 1: Strain Analysis*. Academic Press, London.
Richards, J. R. & Singleton, O. P. 1981. Palaeozoic igneous rocks, ages and their interpretation: Victoria, Australia. *J. geol. Soc. Aust.* **28**, 395–421.
Ridley, J. & Casey, M. 1989. Numerical modeling of folding in rotational strain histories: Strain regimes expected in thrust belts and shear zones. *Geology* **17**, 875–878.
Sanderson, D. J. 1979. The transition from upright to recumbent folding in the Variscan fold belt of southwest England: a model based on the kinematics of simple shear. *J. Struct. Geol.* **1**, 171–180.
Sanderson, D. J. 1982. Models of strain variation in nappes and thrust-sheets: A review. *Tectonophysics* **88**, 201–233.
Sandiford, M. & Keays, R. R. 1986. Structural and tectonic constraints on the origin of gold deposits in the Ballarat Slate Belt, Victoria. In: *Turbidite-hosted Gold Deposits* (edited by Keppie, J. D., Boyle, R. W. & Haynes, S. J.). *Spec. Pap. Geol. Ass. Can.* **32**, 15–24.
Schmid, S. M. 1975. The Glarus overthrust: Field evidence and mechanical model. *Eclog. geol. Helv.* **68**, 247–280.
Shimamoto, T. & Hara, I. 1976. Geometry and strain distribution of single layer folds. *Tectonophysics* **19**, 271–289.
Stephens, M. B., Glassons, M. J. & Keays, R. R. 1979. Structural and chemical aspects of metamorphic layering development in metasediments from Clunes, Australia. *Am. J. Sci.* **279**, 129–160.
Strangward, D. R. 1986. Strain: Methods of determination and application to section reconstruction. Unpublished B.Sc. (Hons.) thesis, Monash University, Melbourne, Australia.
Thomas, D. E., 1939. The structure of Victoria with respect to the Lower Palaezoic rocks. *Min. geol. J. Vict.* **1**, 59–64.
VandenBerg, A. H. M. 1978. The Tasman Fold Belt System. *Tectonophysics* **48**, 267–279.
VandenBerg, A. H. M. 1988. Silurian-Middle Devonian. In: *Geology of Victoria* (2nd edn) (edited by Douglas, J. G. & Ferguson, J. A.). *Victn Div. geol. Soc. Aust.*, 103–146.
Waldron, H. M. & Sandiford, M. 1989. Deformation volume and cleavage development in metasedimentary rocks from the Ballarat Slate Belt. *J. Struct. Geol.* **10**, 53–62.
White, S. H. & Johnston, D. C. 1981. A microstructural study and microchemical study of cleavage lamellae in a slate. *J. Struct. Geol.* **3**, 279–290.
Willman, C. E. 1987. Structural geology of the Bendigo, Castlemaine, Avoca and Inglewood areas and the relationship to gold–quartz mineralisation. Unpublished M.Sc. thesis, Monash University, Melbourne.
Willman, C. E. 1988. Geology of the Spring Gully 1:10,000 map area, Bendigo Goldfield. Report Geol. Surv. Victoria, 1988–1985.
Wood, D. S. 1974. Current reviews of the development of slaty cleavage. *Annu. Rev. Earth & Plant Sci.* **2**, 369–401.
Woodward, N. B., Gray, D. R. & Spears, D. B. 1986. Including strain data in balanced cross-sections. *J. Struct. Geol.* **8**, 313–324.
Woodward, N. B., Wojtal, S., Paul, J. B. & Zadins, Z. Z. 1988. Partitioning of deformation within several external thrust zones of the Appalachian orogen. *J. Geol.* **96**, 351–361.
Wojtal, S. 1986. Deformation within foreland thrust sheets by populations of minor faults. *J. Struct. Geol.* **8**, 341–360.

APPENDIX 1

Table A1. Strain data for the Ballarat Slate Belt (n is the sample size, m is the slope of the regression line ($y = mx + b$) for plots of L_0 vs L_1 for pressure shadows on pyrite, r is the correlation coefficient of the regression line, $1 + e_1$ (X) and $1 + e_3$ (Z) are the maximum and minimum principal stretches respectively, R is the XZ strain ratio, and $S_0 \wedge S_1$ is the bedding–cleavage angle. 'Method' refers either to the strain marker utilized or to the mode of strain determination; FP is framboidal pyrite, E_p is euhedral pyrite, Graps is strain determined from graptolites, and Fry is the Fry method applied to psammites)

Sample No.	Location	n	m	r	$1 + e_1$	$1 + e_3$	R	$S_0 \wedge S_1$	Method
Pelites									
74163	Moorabool River	9	0.66	0.98	1.61	0.62	2.6	20°	FP
74165	Moorabool River	23	0.56	0.99	1.77	0.57	3.1		FP
74167	Moorabool River	2	0.63	1.00	1.58	0.63	2.5	27°	FP
74168	Moorabool River	2	0.64	1.00	1.56	0.64	2.4	14°	FP
74169	Moorabool River	6	0.62	1.00	1.61	0.62	2.6	00°	FP
74170	Moorabool River	13	0.67	0.98	1.49	0.67	2.2	08°	FP
74171	Moorabool River	7	0.60	0.99	1.67	0.60	2.8	00°	FP
84-118	Steiglitz road	4	0.45	0.95	2.20	0.45	4.9	18°	FP
84-119A	Steiglitz road	4	0.53	1.00	1.89	0.53	3.6	45°	FP
84-119C	Steiglitz road	11	0.35	0.99	2.82	0.36	7.9	32°	FP
84-123	Steiglitz road	12	0.36	0.99	2.79	0.36	7.8	18°	FP
85-1	Steiglitz road	8	0.45	0.98	2.20	0.45	4.9	20°	FP
85-3B	Steiglitz road	6	0.33	1.00	3.03	0.33	9.2	10°	FP
95523	Campbelltown						1.55	20°	Graps
96016	Blackwood	3	0.55	0.99	1.80	0.56	3.2	28°	FP
96028	Blackwood	5	0.50	1.00	1.98	0.51	3.8	40°	FP
96020	Blackwood	5	0.48	0.98	2.09	0.48	4.4	35°	FP
95988	Tyrconnel Mine	3	0.58	1.00	1.74	0.58	3.0		FP
96009	Tyrconnel Mine	4	0.64	0.94	1.56	0.64	2.4	18°	EP
96038	Tyrconnel Mine	3	0.46	1.00	2.18	0.46	4.7	45°	FP
89-281	Daylesford	1	—	—	1.8	0.56	3.2	32°	FP
95512	Bullarto				1.16		1.55	23°	Graps
84-137	Castlemaine	7	0.26	0.98	3.85	0.26	14.8	18°	EP
84-131(S)	East Bendigo	5	0.17	0.99	5.81	0.17	34.2	08°	EP
84-131(P)	East Bendigo	2					50.8	08°	EP
84-126	Bendigo	5	0.34	0.99	2.95	0.34	8.7		EP
84-130	Bendigo	11	0.32	0.98	3.13	0.32	9.8	15°	FP
84-130A	Bendigo	3	0.33	1.00	3.03	0.33	9.2	15°	FP
22795	Bendigo	2	0.5	1.00	2.00	0.50	4.0	35°	FP
22796	Bendigo	4	0.38	0.97	2.63	0.38	6.9		EP
87-45	Lake Eppalock	12	0.56	0.99	1.78	0.56	3.2		FP
95514	Mia Mia				1.16	0.86	1.55		Graps
88-197	Heathcote	4					32.7	10°	EP
	Ingliston				2.37	0.65	3.7		Graps
84-19Da	Lerderderg Gorge	5	0.70	1.00	1.43	0.70	2.0	15°	FP
84-19Db	Lerderderg Gorge	7	0.57	1.00	1.75	0.57	3.1	15°	FP
84-19F	Lerderderg Gorge	5	0.44	0.99	2.27	0.44	5.2	50°	FP
TM2	Lerderderg Gorge	2	0.52	1.00	1.92	0.52	3.7	13°	FP
TM2a	Lerderderg Gorge	6	0.30	0.99	3.33	0.30	11.1	13°	FP
CT7A	Lerderderg Gorge	7	0.34	1.00	2.94	0.34	8.7	20°	FP
CT5A	Lerderderg Gorge	5	0.26	0.99	3.85	0.26	14.8	10°	FP
Psammites									
96011	Blackwood						1.3		Fry
96012	Blackwood						1.7		Fry
96023	Blackwood						1.6		Fry
96043	Tyrconnel Mine						1.3		Fry
96007	Tyrconnel Mine						1.6		Fry
95995	Tyrconnel Mine						1.7		Fry
96037	Tyrconnel Mine	3	0.79	1.00	1.26	0.79	1.6	60°	EP
95992	Tyrconnel Mine	3	0.76	1.00	1.32	0.76	1.7	34°	EP
84-134	Bendigo	2	0.88	1.00	1.13	0.89	1.3		EP
	Clunes	1	—	—	1.15	0.87	1.3		EP

N.B. Data from Blackwood and Tyrconnel Mine are from Kirchner (1987).

APPENDIX 2

Strain analysis methods: pressure shadows

(1) *Pyrites with straight fibres.* The Pyrite method (Durney & Ramsay 1973) was used to determine the maximum principal stretch $(1 + e_1)$ in samples containing pyrite. The stretch $(1 + e_1)$ is given by:

$$1 + e_1 = (L_1 - L_0)/L_0,$$

where L_1 is the fibre length + pyrite radius (measured in the direction of the fibres) and L_0 is the pyrite radius (measured in the direction of the fibres). As many pressure shadows as possible were measured, but low numbers of pyrites in some of the samples necessitated sample sizes less than 5 (see Appendix 1). The reliability of the data was checked graphically and it was found that as few as two or three measurements generally gave a reasonable approximation of the strain. Graphs of L_1 vs L_0 for all samples define linear arrays with zero y intercepts ($b \approx 0$) and varying slopes (m) which are a function of the stretch (see Appendix 1).

Representative stretches $(1 + e_1)$ were determined from the regression line equations ($y = mx + b$ form; see Appendix 1). The minimum principal stretch $(1 + e_3)$ was taken as $1/(1 + e_1)$ since the deformation approximates plane strain and constant volume. In most cases the data defined linear arrays with strong correlation (i.e. $r > 0.97$). Data points more than 2δ (standard deviations) removed from the line were not included in the regression line calculations. These tended to be over-long pressure shadows on larger pyrites.

(2) *Pyrites with curved fibres.* The principal incremental extensional strain (e_{1n}) has been calculated using the Pyrite method (Durney & Ramsay 1973, p. 92, Gray & Durney 1979), assuming the fibres are parallel to the incremental extensions in the rock and that there is no relative rigid-body rotation between the shadow, pyrite and matrix. The presence of ghost-fibre inclusion trails/partition lines (Fig. 5) were used to calculate the incremental strain history and the total XZ strains as these appeared to trace out the displacement path of the external boundary as it was drawn away from the pyrite (see Ramsay & Huber 1983, p. 269). Serial incremental extension graphs (Fig. 11) from several pressure shadows within individual samples can be used to test the uniformity of sequences of incremental extensions and to check for differences caused by potential body rotations of these euhedral pyrite with their inequant shapes (see insets Fig. 11).

The cleavage orientation in the final state was used as the reference orientation. This orientation defines a coordinate system fixed to the pyrite which coincides with the cleavage trace in the final state (cf. Gray & Durney 1979). As such the coordinate system moves with the body of the rock, and the calculated strains register the internal deformation and not the body rotations and translations of the rock. The total strains (Appendix 1, 88-197 and 84-131) have been calculated with $e_{2n} = 0$ and $e_{3n} = 1/(1 + e_{1n})$. This is reasonable given the relations discussed previously (see Table 2).

Strain analysis methods: graptolites

Determination of bulk total strains from graptolites in the Ballarat Slate Belt was either done by (1) investigating variation in thecal angle with stipe orientation in the bedding plane for a particular species of graptolite (see Ramsay & Huber 1983, pp. 136–140) or (2) investigating thecal spacing in the deformed and undeformed states, where spacing in the deformed state was determined in graptolites whose stipes were parallel and perpendicular to the bedding–cleavage intersection trace on the bedding surface (Hills & Thomas 1944). Bulk rock strains were estimated using graptolite strains, which represent stretches $(1 + e)$ in bedding, from samples with different bedding–cleavage angles (or θ' assuming that the cleavage approximates the XY plane of the strain ellipsoid). Best-fit ellipses were constructed from polar graph plots of stretch $(1 + e)$ vs orientations θ' for different samples from a given exposure where bedding–cleavage angle varied due to folding. In that sense these strains are truly estimates of the bulk rock strain at the scale of individual folds.

Strain analysis methods: psammites

Quartz grain distributions in sandstones were investigated by the Fry method (Fry 1979, Ramsay & Huber 1983, pp. 111–113) using photomicrographs of thin sections.